

# Sensor Project 1

Autonomous Intelligent Systems

- Report -

Start of project: 29/10/2021

Submission date: 27/04/2022

Project supervisors: Prof. P. Nauth / Prof. A. Pech

Project coordinator: Mr. J. Umansky

**Group 1:**

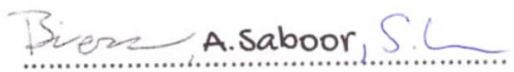
Tobias Biermann 1207763 | Sascha Kotzian 1207378 | Saboor Abdul 1322460

## Affirmation

We declare that we have authored this report independently, that we have not used other than the declared sources / resources, and that we have explicitly marked all material which has been quoted either literally or by content from the used sources.

27/04/2022  
.....

date

A. Saboor, S.L.

(signatures)

## Table of contents

Affirmation .....	I
Table of contents.....	II
List of figures .....	IV
List of tables .....	IX
List of abbreviations .....	X
1    Introduction.....	1
2    State of the art (SOTA) .....	2
2.1    Analysis of obstacle detection using ultrasonic sensor .....	2
2.2    Ultrasonic sensor-based human detector using Oneclass classifiers.....	2
2.3    An US for human presence detection to assist rescue work in large buildings .....	3
3    Task & relation to the module .....	4
4    Theoretical background .....	5
4.1    Ultrasonic sensor .....	5
4.2    Features .....	6
4.3    Standardisation of the data .....	7
4.4    Neighborhood Component Analysis (NCA) .....	8
4.5    Coarse Gaussian SVM .....	8
5    Evaluation of 1 <sup>st</sup> data set.....	9
6    Threshold adjustment .....	12
6.1    Variations of both features.....	12
6.2    Variations of X value (Constant Y value) .....	14
7    Evaluation of 2 <sup>nd</sup> data set.....	16
8    Variation of seat position .....	18
9    Evaluation of different objects.....	22
10   Machine Learning Classification.....	24

10.1	Feature Extraction.....	25
10.2	Feature Selection .....	25
10.2.1	Neighborhood Component Analysis (NCA) .....	25
10.2.2	Correlations .....	27
10.3	Decision making .....	27
11	Summary and outlook.....	31
	List of references .....	XI
	Appendix.....	XIV

## List of figures

<b>Figure 1:</b> Distance of the vehicle from the obstruction [2, Chart-1].....	2
<b>Figure 2:</b> Elementary Functional Diagram of data processing of sensor [6, p. 3].....	4
<b>Figure 3:</b> Ultrasonic sensor working diagram [7, Figure 3] .....	5
<b>Figure 4:</b> Confusionmatrix, TPR and FNR of the first data set .....	10
<b>Figure 5:</b> Accuracies of events independent of human and t-shirt .....	11
<b>Figure 6:</b> Accuracies of the first threshold measurements.....	12
<b>Figure 7:</b> Accuracies of the second threshold measurements.....	13
<b>Figure 8:</b> Confusion matrix of thresholds X140 Y12000.....	14
<b>Figure 9:</b> Accuracies of the third threshold measurements .....	15
<b>Figure 10:</b> Confusionmatrix, TPR and FNR of the second data set .....	16
<b>Figure 11:</b> Comparison of the events of the first and second data set .....	17
<b>Figure 12:</b> States, angles and distances for seat position front.....	19
<b>Figure 13:</b> States, angles and distances for seat position front.....	19
<b>Figure 14:</b> Accuracy of different objects .....	22
<b>Figure 15:</b> Confusionmatrix of test data set (sensor classification).....	24
<b>Figure 16:</b> Neighborhood Component Analysis of training data set .....	26
<b>Figure 17:</b> Correlation matrix of the different features.....	27
<b>Figure 18:</b> Exemplary classification with the help of two features.....	28
<b>Figure 19:</b> Confusionmatrix of test data set (MLM classification) .....	30
<b>Figure 20:</b> Measurement with no passenger .....	XIV
<b>Figure 21:</b> Normal Sitting RT Saboor.....	XIV
<b>Figure 22:</b> Reverse Sitting RT Saboor .....	XIV
<b>Figure 23:</b> Seatbelt RT Saboor.....	XIV
<b>Figure 24:</b> Movements RT Saboor.....	XV
<b>Figure 25:</b> Folded arms RT Saboor .....	XV
<b>Figure 26:</b> Towel RT Saboor .....	XV
<b>Figure 27:</b> Normal Sitting GT Saboor.....	XV
<b>Figure 28:</b> Reverse Sitting GT Saboor .....	XVI
<b>Figure 29:</b> Seatbelt GT Saboor .....	XVI
<b>Figure 30:</b> Movements GT Saboor .....	XVI
<b>Figure 31:</b> Folded arms GT Saboor .....	XVI

<b>Figure 32:</b> Towel GT Saboor .....	XVII
<b>Figure 33:</b> Normal Sitting JWT Tobias .....	XVII
<b>Figure 34:</b> Reverse Sitting JWT Tobias .....	XVII
<b>Figure 35:</b> Seatbelt JWT Tobias .....	XVII
<b>Figure 36:</b> Movements JWT Tobias .....	XVIII
<b>Figure 37:</b> Folded arms JWT Tobias .....	XVIII
<b>Figure 38:</b> Towel JWT Tobias.....	XVIII
<b>Figure 39:</b> Normal Sitting BT Tobias.....	XVIII
<b>Figure 40:</b> Reverse Sitting BT Tobias .....	XIX
<b>Figure 41:</b> Seatbelt BT Tobias.....	XIX
<b>Figure 42:</b> Movements BT Tobias.....	XIX
<b>Figure 43:</b> Folded arms BT Tobias .....	XIX
<b>Figure 44:</b> Towel BT Tobias .....	XX
<b>Figure 45:</b> Normal Sitting WT Tobias .....	XX
<b>Figure 46:</b> Reverse Sitting WT Tobias.....	XX
<b>Figure 47:</b> Seatbelt WT Tobias .....	XX
<b>Figure 48:</b> Movements WT Tobias .....	XXI
<b>Figure 49:</b> Folded arms WT Tobias.....	XXI
<b>Figure 50:</b> Towel WT Tobias .....	XXI
<b>Figure 51:</b> Normal Sitting TT Tobias .....	XXI
<b>Figure 52:</b> Reverse Sitting TT Tobias .....	XXII
<b>Figure 53:</b> Seatbelt TT Tobias .....	XXII
<b>Figure 54:</b> Movements TT Tobias.....	XXII
<b>Figure 55:</b> Folded arms TT Tobias .....	XXII
<b>Figure 56:</b> Towel TT Tobias.....	XXIII
<b>Figure 57:</b> Normal Sitting GT Sascha .....	XXIII
<b>Figure 58:</b> Reverse Sitting GT Sascha .....	XXIII
<b>Figure 59:</b> Seatbelt GT Sascha .....	XXIII
<b>Figure 60:</b> Movements GT Sascha .....	XXIV
<b>Figure 61:</b> Folded arms GT Sascha .....	XXIV
<b>Figure 62:</b> Towel GT Sascha.....	XXIV
<b>Figure 63:</b> Threshold Measurement 1 Saboor .....	XXV

<b>Figure 64:</b> Threshold Measurement 1 Tobias .....	XXV
<b>Figure 65:</b> Confusion matrix of thresholds X160 Y12000.....	XXV
<b>Figure 66:</b> Confusion matrix of thresholds X160 Y14000.....	XXVI
<b>Figure 67:</b> Confusion matrix of thresholds X160 Y16000.....	XXVI
<b>Figure 68:</b> Confusion matrix of thresholds X160 Y20000.....	XXVII
<b>Figure 69:</b> Confusion matrix of thresholds X180 Y10000.....	XXVII
<b>Figure 70:</b> Confusion matrix of thresholds X180 Y12000.....	XXVIII
<b>Figure 71:</b> Confusion matrix of thresholds X180 Y14000.....	XXVIII
<b>Figure 72:</b> Confusion matrix of thresholds X200 Y10000.....	XXIX
<b>Figure 73:</b> Confusion matrix of thresholds X200 Y12000.....	XXIX
<b>Figure 74:</b> Confusion matrix of thresholds X200 Y14000.....	XXX
<b>Figure 75:</b> Threshold measurement 2&3 Saboor.....	XXX
<b>Figure 76:</b> Threshold measurement 2&3 Tobias.....	XXX
<b>Figure 77:</b> Threshold measurement 2&3 Sascha .....	XXXI
<b>Figure 78:</b> Confusion matrix of thresholds X120 Y12000.....	XXXI
<b>Figure 79:</b> Confusion matrix of thresholds X140 Y10000.....	XXXII
<b>Figure 80:</b> Confusion matrix of thresholds X140 Y14000.....	XXXII
<b>Figure 81:</b> Confusion matrix of thresholds X160 Y12000.....	XXXIII
<b>Figure 82:</b> Confusion matrix of thresholds X10 Y1000.....	XXXIII
<b>Figure 83:</b> Confusion matrix of thresholds X30 Y1000.....	XXXIV
<b>Figure 84:</b> Confusion matrix of thresholds X50 Y1000.....	XXXIV
<b>Figure 85:</b> Confusion matrix of thresholds X70 Y1000.....	XXXV
<b>Figure 86:</b> Confusion matrix of thresholds X90 Y1000.....	XXXV
<b>Figure 87:</b> Confusion matrix of thresholds X110 Y1000.....	XXXVI
<b>Figure 88:</b> Confusion matrix of thresholds X130 Y1000.....	XXXVI
<b>Figure 89:</b> Confusion matrix of thresholds X150 Y1000.....	XXXVII
<b>Figure 90:</b> Confusion matrix of thresholds X170 Y1000.....	XXXVII
<b>Figure 91:</b> Confusion matrix of thresholds X190 Y1000.....	XXXVIII
<b>Figure 92:</b> Confusion matrix of thresholds X210 Y1000.....	XXXVIII
<b>Figure 93:</b> Confusion matrix of thresholds X230 Y1000.....	XXXIX
<b>Figure 94:</b> Percentage differences of events between the data sets Saboor .....	XXXIX
<b>Figure 95:</b> Percentage differences of events between the data sets Tobias (Part 1).....	XL

<b>Figure 96:</b> Percentage differences of events between the data sets Tobias (Part 2).....	XL
<b>Figure 97:</b> Percentage differences of events between the data sets Sascha .....	XLI
<b>Figure 98:</b> Empty SPF SF .....	XLI
<b>Figure 99:</b> Empty SPF SN .....	XLI
<b>Figure 100:</b> Empty SPF SB.....	XLII
<b>Figure 101:</b> Empty SPB SF.....	XLII
<b>Figure 102:</b> Empty SPB SN .....	XLII
<b>Figure 103:</b> Empty SPB SB .....	XLII
<b>Figure 104:</b> Tobias SPF SF.....	XLIII
<b>Figure 105:</b> Tobias SPF SN .....	XLIII
<b>Figure 106:</b> Tobias SPF SB.....	XLIII
<b>Figure 107:</b> Tobias SPB SF.....	XLIII
<b>Figure 108:</b> Tobias SPB SN .....	XLIV
<b>Figure 109:</b> Tobias SPB SB .....	XLIV
<b>Figure 110:</b> Sascha SPF SF .....	XLIV
<b>Figure 111:</b> Sascha SPF SN.....	XLIV
<b>Figure 112:</b> Sascha SPF SB .....	XLV
<b>Figure 113:</b> Sascha SPF SN.....	XLV
<b>Figure 114:</b> Sascha SPB SN .....	XLV
<b>Figure 115:</b> Sascha SPB SB.....	XLV
<b>Figure 116:</b> Confusion matrix of SPF SF sensor 1.....	XLVI
<b>Figure 117:</b> Confusion matrix of SPF SN sensor 1 .....	XLVI
<b>Figure 118:</b> Confusion matrix of SPF SB sensor 1 .....	XLVII
<b>Figure 119:</b> Confusion matrix of SPB SF sensor 1 .....	XLVII
<b>Figure 120:</b> Confusion matrix of SPB SN sensor 1.....	XLVIII
<b>Figure 121:</b> Confusion matrix of SPB SB sensor 1 .....	XLVIII
<b>Figure 122:</b> Confusion matrix of SPF SF sensor 2.....	XLIX
<b>Figure 123:</b> Confusion matrix of SPF SN sensor 2 .....	XLIX
<b>Figure 124:</b> Confusion matrix of SPF SB sensor 2 .....	L
<b>Figure 125:</b> Confusion matrix of SPB SF sensor 2 .....	L
<b>Figure 126:</b> Confusion matrix of SPB SN sensor 2 .....	LI
<b>Figure 127:</b> Confusion matrix of SPB SB sensor 2 .....	LI

<b>Figure 128:</b> Plastic Baby .....	LII
<b>Figure 129:</b> Backpack 1.....	LII
<b>Figure 130:</b> Backpack 2.....	LII
<b>Figure 131:</b> Cardboard box.....	LII
<b>Figure 132:</b> Traffic cones .....	LIII

## List of tables

<b>Table 1:</b> Classification based on TDF[3, Table 2].....	3
<b>Table 2:</b> Classification based on FDF[3, Table 4].....	3
<b>Table 3:</b> Events with passengers .....	9
<b>Table 4:</b> Heights of the participants.....	9
<b>Table 5:</b> Horizontal states .....	18
<b>Table 6:</b> Lateral states .....	18
<b>Table 7:</b> Seat position evaluation sensor 1 .....	19
<b>Table 8:</b> Seat position evaluation sensor 2 .....	19
<b>Table 9:</b> Distances of different objects .....	23
<b>Table 10:</b> The seven most important features based on NCA .....	26
<b>Table 11:</b> Comparison of the five best classifiers .....	29
<b>Table 12:</b> Comparison of the 25 classifiers .....	LIV

## List of abbreviations

ACCTEST	Accuracy test
ACCVAL	Accuracy validation
BT	Black t-shirt
DAQ	Data acquisition
EMG	Electromyography
FA	Folded arms
FFT	Fast Fourier Transform
FNR	False negative rate
GT	Green t-shirt
GUI	Graphical User Interface
JWT	Just white t-shirt
KNN	k-nearest-neighbours
M	Movements
MB	Megabyte
MLM	Machine learning model
MS	Memory space
NCA	Neighborhood Component Analysis
NN	Neural network
NS	Normal sitting
Pred.	Prediction
PS	Prediction speed
ReLU	Rectified linear unit
RT	Red t-shirt
S	Seatbelt
SB	Backrest on the rear bench & angle greater than 90 degrees
SF	Backrest turned forwards & angle smaller than 90 degrees
SM	Spectral Measurements
SN	Backrest straight & angle approx. 90 degrees
SPB	Max. horizontal distance between seat and sensor
SPF	Min. horizontal distance between seat and sensor
SVM	Support-Vector-Machine
T	Towel (around the neck)
TPR	True positive rate
Tt	Training time
TT	Tanktop
UAS	University of Applied Sciences
US	Ultrasonic
WT	White t-shirt

## 1 Introduction

The rapid advancement of artificial intelligence and machine learning in industry means that sensor technology continues to advance in terms of intelligent detection. Due to a large amount of available data today, intelligent systems are being used in a wide range of applications. Sensors based on data-driven algorithms are present in the fields of intelligent transport, autonomous vehicles/robots, wearable computers and many more. Traditional approaches to sensing are being challenged by significant performance improvements in terms of resource optimisation combined with low financial costs [1].

The aim of this work is to perform a reliability test of an existing ultrasonic sensor system that distinguishes between an empty seat and a person in the car. With the help of different parameter adjustments and aspects of supervised learning, an improvement of the detection rates will be investigated. The results of this work could be integrated into the existing system to improve its performance.

In the context of this work, the current state of the art is first explained in more detail on the basis of comparable projects as well as the task including the relation to the module “Autonomous Intelligent Systems”. Furthermore, the theoretical foundations for understanding this work are described.

This is followed by the evaluation of two data sets based on different parameter settings. Chapters 8 and 9 analyse the influence of different seating positions and objects. Finally, a machine learning model is created, which contains all the necessary steps from the extraction of features to the selection of a suitable classification algorithm. In addition to the classification algorithm, other factors are discussed with regard to a resource-optimising integration into the existing sensor system.

## 2 State of the art (SOTA)

In this chapter, the current state of the art is explained in more detail on the basis of three studies. The studies are based on similar topics as in this report, such as the recognition of different objects or people with the help of ultrasonic sensors.

### 2.1 Analysis of obstacle detection using ultrasonic sensor

The 2017 study “Analysis of obstacle detection using ultrasonic sensor” investigates the distance measurement of various objects using an ultrasonic sensor in a vehicle and the classification of objects with the help of a neural network. The objects are made of wood, paper, fabric, plastic and metal. Regarding the distance measurement, there is a high correlation coefficient between all materials except fabric which can be seen in the following figure:

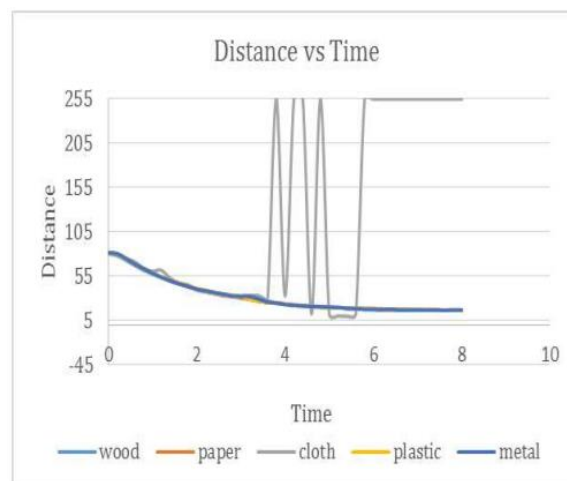


*Figure 1: Distance of the vehicle from the obstruction [2, Chart-1]*

With regard to the classification of the materials using the neural network, the authors have achieved low accuracies, which is due to similar patterns of the different materials. Therefore, the results of the study are that using the ultrasonic sensor, distance measurement of the materials is feasible, but the different materials cannot be classified in the process [2].

### 2.2 Ultrasonic sensor-based human detector using Oneclass classifiers

The study published in 2015 called “Ultrasonic sensor-based human detector using Oneclass classifiers” is about the creation of a human recognition system based on ultrasonic sensors and fuzzy rules. The environment for this is a coffee shop where it is to distinguish between the detection of a human being and various objects like doors, chairs and glass. With the help

of the fuzzy rules and the extraction of different features from the time and frequency domain, the authors achieve high accuracies with regard to the recognition of a human being, as can be seen in the following tables [3]:

*Table 1: Classification based on TDF[3, Table 2]*

	<i>Object</i>	<i>Human</i>
Wooden door	20	0
Glass door	7	13
Cushioned chair	19	1
Human	5	65

*Table 2: Classification based on FDF[3, Table 4]*

	<i>Object</i>	<i>Human</i>
Wooden door	20	0
Glass door	15	5
Cushioned chair	20	0
Human	8	62

## 2.3 An US for human presence detection to assist rescue work in large buildings

This study is based on the idea of using ultrasonic sensors to locate people in a burning building so that emergency services can find them quickly. With the help of a 3D model into which different characteristics of a person can be fed, a running person crossing the ultrasonic sensor is simulated. The data is then converted into a spectrogram, which by means of an algorithm gives probabilities for the detection of a running person. It is shown that optimal detections occur at a radius of 4 metres and these are independent of the smoke development in a room [4].

### 3 Task & relation to the module

The ultrasonic sensor provided by Frankfurt UAS is, by definition, an autonomous system or an intelligent system, as it can make decisions about a classification based on machine learning, in this case empty seat or with person. In relation to the process of an autonomous system, the sensor is usually first used to analyse the current state of the environment with its information. This step is also called perception. In robotics, this information is used to plan the shortest or best path with the help of a computer (cognition). The actuators of the robot or autonomous system are then optimally controlled [5]. Since in this case we are dealing exclusively with an intelligent system or sensor, the process from receiving the ultrasonic signals to making the decision is as shown in the following figure:

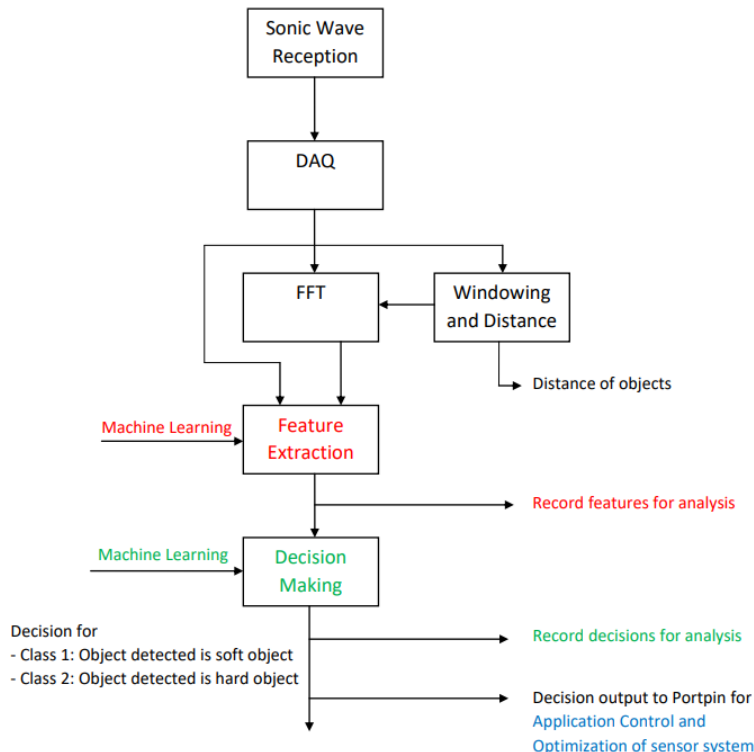


*Figure 2: Elementary Functional Diagram of data processing of sensor [6, p. 3]*

This process is based on supervised learning, because it is not only about finding clusters or patterns in the data, but also about making a decision about an empty seat or a person in the car. Consequently, chapters 5-9 analyse and evaluate the classification results of the sensor in relation to different application procedures. This includes the evaluation of the influence of different persons, thresholds, seating positions and objects. In chapter 10, the process described here is used as a basis for the creation of a machine learning model, which should achieve a higher accuracy in the recognition of the classes than the sensor of the Frankfurt UAS.

## 4 Theoretical background

In this chapter, the theoretical foundations of this thesis are explained in more detail. In addition to explaining how an ultrasound sensor works, various machine learning factors are described. This includes the presentation of the most important features for feature extraction as well as a Neighborhod Component Analysis for feature selection. Finally, the importance of standardising the data and the classification algorithm used in this work, namely Coarse Gaussian SVM, is illustrated.

### 4.1 Ultrasonic sensor

The basis of an ultrasonic sensor is the periodic emission of ultrasonic pulses around a frequency of approx. 40 kHz. The ultrasonic waves propagate in the medium, in this case air, and are reflected by the object. The latter are also called echoes. Since the speed of propagation corresponds to the speed of sound at room temperature and the ultrasonic waves travel once the distance to the object and back, the distance between the ultrasonic probe and the object can be determined using the following formula:

$$distance = \frac{c_s * t}{2} \quad (4.1)$$

Where  $c_s$  is the speed of sound and  $t$  is the time that elapses between the emission of the signal and its reception at the sensor. A microcontroller is built into the sensor to read out the data from the sensor and then process the data further. This transforms the system from an ultrasonic sensor into an intelligent system. The complete experimental setup is shown in the following figure as an example [7, p.1-3]:

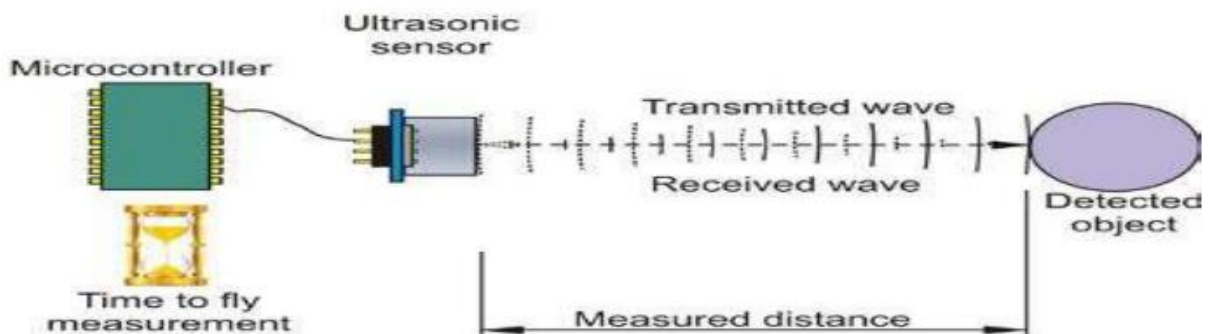


Figure 3: Ultrasonic sensor working diagram [7, Figure 3]

## 4.2 Features

In this section, the properties of the features used in this work are described in more detail. The features are from the fields of statistics, spectral properties of a signal and electromyography. For later analysis, the features are given index numbers. In addition, the name of each feature is followed by a mathematical or general description. The following table summarises the most important information:

<i>Index</i>	<i>Name</i>	<i>Area</i>	<i>Description</i>
<b>1</b>	Standard deviation	Statistics	$\sigma = \sqrt{\frac{1}{N-1} \sum_{n=1}^N (x_n - \mu)^2}$
<b>2</b>	Max. value	Statistics	$x_{max} = \max x_n $
<b>3</b>	Band power	SM	average power of the signal
<b>4</b>	Equivalent noise bandwidth	SM	$x_{enbw} = \frac{\sum_n  w_n ^2}{ \sum_n w_n ^2}$
<b>5</b>	Occupied bandwidth	SM	Frequency difference between two data points where integrated power crosses 0.5% and 99.5% of the signal
<b>6</b>	Power bandwidth	SM	3-dB (half-power) bandwidth of the signal
<b>7</b>	Signal to noise and distortion ratio	SM	$x_{SINAD} = \frac{P_S + P_N + P_D}{P_N + P_D}$
<b>8</b>	Signal to noise ratio	SM	$x_{SNR} = \frac{P_S}{P_N}$
<b>9</b>	Max. to Min. difference	Statistics	$x_{p2p} = \max x_n  - \min x_n$
<b>10</b>	Crest Factor	Statistics	$x_{crest} = \sqrt{\frac{x_p}{\frac{1}{N} \sum_{n=1}^N x_n^2}}$
<b>11</b>	Root-mean-square	Statistics	$x_{rms} = \sqrt{\frac{\sum x_n^2}{N}}$
<b>12</b>	Mean	Statistics	$\mu = \frac{1}{N} \sum_{n=1}^N x_n$

<b>13</b>	Kurtosis	Statistics	$x_{kurt} = \frac{\frac{1}{N} \sum_{n=1}^N (x_n - \mu)^4}{\left[ \frac{1}{N} \sum_{n=1}^N (x_n - \mu)^2 \right]^2}$
<b>14</b>	Skewness	Statistics	$x_{skew} = \frac{\frac{1}{N} \sum_{n=1}^N (x_n - \mu)^3}{\left[ \frac{1}{N} \sum_{n=1}^N (x_n - \mu)^2 \right]^{\frac{3}{2}}}$
<b>15</b>	Min. value	Statistics	$x_{min} = \min x_n $
<b>16</b>	Enhanced Wavelength	EMG	$x_{EWL} = \sum_{n=2}^N  (x_n - x_{n-1})^p $ $p = \begin{cases} 0.75, & \text{if } n \geq 0.2N \text{ and } n \leq 0.8N \\ 0.5, & \text{otherwise} \end{cases}$
<b>17</b>	Log Teager Kaiser Energy Operator	EMG	$x_{LTKEO} = \log \left( \sum_{n=0}^{N-2} {x_n}^2 - x_{n-1} * x_{n+1} \right)$
<b>18</b>	Max. Fractal Length	EMG	$x_{MFL} = \log_{10}(\sqrt{[x_{n+1} - x_n]^2})$

The list of features is based on the evaluations of the following literature [8, p. 5-6], [9], [10], [11], [12], [13], [14, p. 86], [15, p. 1823], [16].

#### 4.3 Standardisation of the data

Since the input features are based on different value scales after extraction, a direct comparison in feature selection is not possible. When entering features of different value scales, biased accuracies of the machine learning model could occur. To solve this problem, the data can be standardised using a z-score transformation. Another advantage is that standardised data sets are often the prerequisite for various distance-based classification algorithms such as SVM. Standardisation rescales each feature linearly with a standard deviation of 1 and an arithmetic mean of 0 [17], [18, p. 425]:

$$z = \frac{x - \mu}{\sigma} \quad (4.2)$$

A more detailed explanation of standardisation can be found in the following literature [19, p. 26-32].

#### 4.4 Neighborhood Component Analysis (NCA)

NCA is based on the Nearest-Neighbour algorithm and is used to weight features in a dataset. The weighting is done by maximising the expected leave-one-out classification accuracy, which also contains a regularisation term. In addition, NCA is suitable for multi-class problems and no preconditions are imposed on the distributions of the data. The Nearest-Neighbour classification is optimised so that a suitable feature vector  $w$  is determined for each feature. This is based on the distances of the data points and can be expressed with the following formula:

$$D_w(x_i, x_j) = \sum_{l=1}^d w_l^2 |x_{il} - x_{jl}| \quad (4.3)$$

Where  $x_i$  and  $x_j$  describe two data points,  $d$  is the number of features and  $w_l$  is the weighting for each  $i$ -th feature [20, p. 161-162]. For a more detailed derivation including the leave-one-out accuracy mentioned above, please refer to the following literature [20].

#### 4.5 Coarse Gaussian SVM

In general, the principle of an SVM classifier is based on support vectors with which an optimal hyperplane is formed to maximise the distance between two classes by means of a gradient descent. SVM algorithms can be used for both classification and regression problems. For non-linear classification problems, such as the one presented in this paper, the so-called kernel function can be modified [21]. In this algorithm, a Gaussian kernel is used which reads as follows:

$$K(X, X_i) = e^{-Y|X-X_i|^2} \quad (4.4)$$

Here  $X$  and  $X_i$  are input vectors,  $|X - X_i|$  is the euclidean distance between the two input vectors and  $Y$  is the kernel scale parameter, which must always be greater than zero. The kernel scale parameter for the Coarse Gaussian SVM algorithm can be calculated with the following formula:

$$Y = 4 * \sqrt{n} \quad (4.5)$$

Where  $n$  is the number of features selected [22, p. 8,11]. The last important parameter is the box constraint level. This is set to 1 in this algorithm. This parameter controls the maximum penalty for data points that lie outside a certain range, which should prevent overfitting, for example [23].

## 5 Evaluation of 1<sup>st</sup> data set

In this chapter, the procedure for creating the first data set and the corresponding evaluations is explained in more detail. According to the task, a number of 10 people should get into the car. However, this is not possible due to the current pandemic. Therefore, the first data set is based on the group members performing 6 different events while sitting in the car. The events and the heights of the participants are listed in the following table:

Events	Participant	Height
Normal Sitting	Sabbor Abdul	1,71m
Reverse Sitting		
Seatbelt	Sascha Kotzian	1,75m
Movements		
Towel (around the neck)	Tobias Biermann	1,85m
Folded Arms		

*Table 3: Events with passengers*

*Table 4: Heights of the participants*

The six events are performed with seven different summer clothes. Mainly short-sleeved t-shirts in different colours and a tank top are worn. This results in a total of 42 possibilities to get into the car. For each event, 500 FFT spectra are recorded and the classes are stored to obtain meaningful results. For the first data set, the standard thresholds for the features number 1 and 10 are used. In order to obtain an evenly distributed data set, 21.000 measurements are also taken without anyone sitting in the car. This means that 42.000 measurements are included in the confusion matrix. Between the individual events, the same number of measurements are always carried out with an empty seat, as it has been shown that the sensor usually needs a short time to adjust to a certain class.

The car seat is adjusted so that there is the maximum horizontal distance between the participant and the sensor. The angle of the car seat or backrest is set to 90 degrees, so that in combination with the horizontal seat position, this results in a distance between the seat and the sensor of 0.98 metres. The pictures of the individual events taken at the university can be found in the appendix from *Figure 20* to *Figure 62*. The confusion matrix for the first data set can be seen in the following figure:

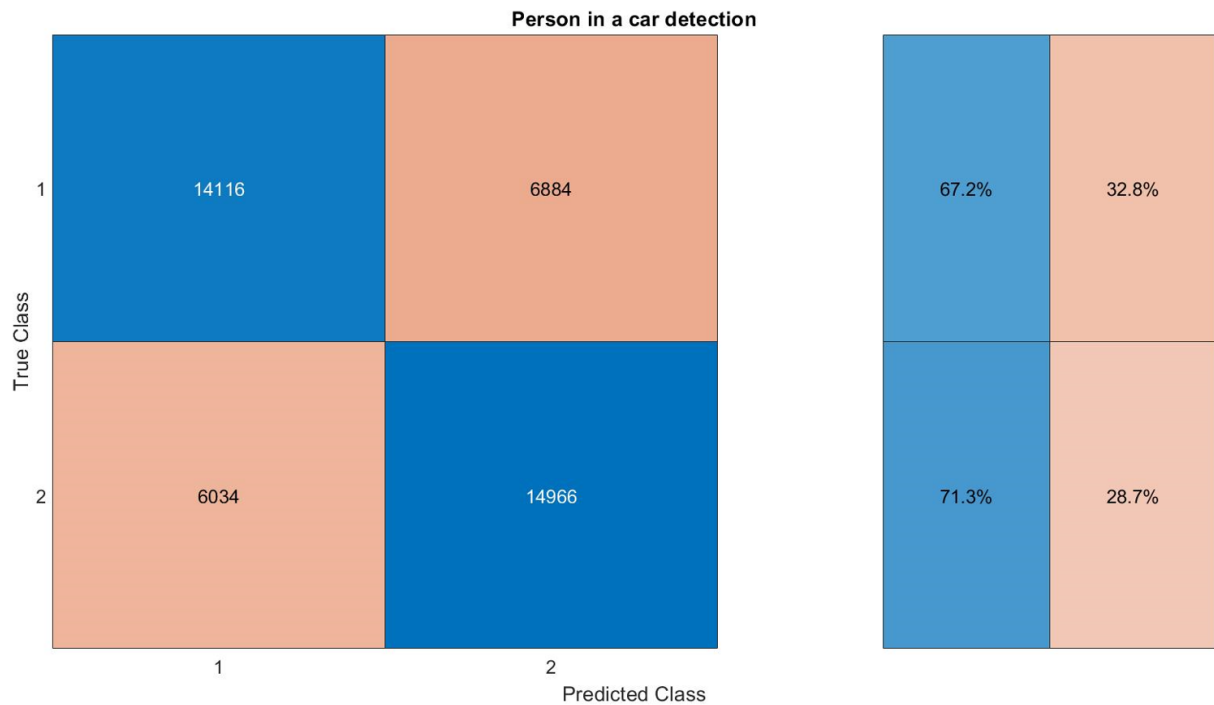


*Figure 4: Confusionmatrix, TPR and FNR of the first data set*

Class 1 refers to the detection of a car seat and class 2 to the detection of a person. On the left side of the figure, the absolute values of correctly and incorrectly predicted classes can be seen. On the right side the so-called True Positive Rates (left blue column) and the False Negative Rates (right red column) in relation to the two classes are shown. The correctly predicted values are very close for both classes. To get a better understanding of which events have the greatest impact on correctly predicted classes, another statistic can be used. However, this statistic can only be used for the detection of the second class, as only here different events of a class are simulated. The following figure shows the accuracies of the different events regardless of the t-shirt worn and the person:

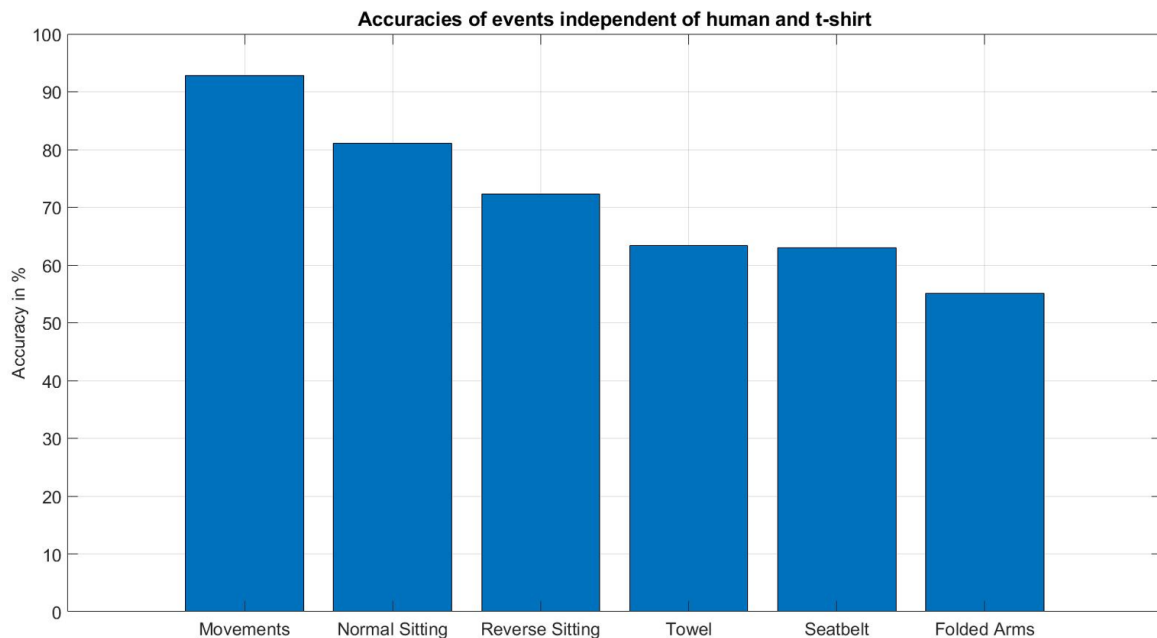


*Figure 5: Accuracies of events independent of human and t-shirt*

Regardless of the t-shirt worn, the figure clearly shows that the events "Movements" and "Normal Sitting" are the decisive factors for a high true positive rate. In addition, these factors vary least with respect to different people in the car and clothing worn. The "Reverse Sitting" factor also generally shows a good detection rate, but is very dependent on how a person sits reverse in a car. Possible reasons for the low detection rates of the last three events could be that the sensor incorrectly detects class 1 due to the towel, the seatbelt or the wristbands or watches on the arm, as the ultrasonic waves are reflected with respect to this class.

## 6 Threshold adjustment

In order to achieve higher true positive and false negative rates in the next dataset, the features number 1 and 10 of the ultrasonic sensor are systematically varied in the following chapter. The variation of the thresholds is based on the goal to better detect a person sitting normally in the car and an empty seat. In this case the event "Normal Sitting" is the reference for all other events, as the latter is the basis for many events such as "Seatbelt", "Towel (around the neck)" or "Folded Arms". The features are the same as the X and Y values, which can be adjusted in the GUI. Analogous to the first data set, the maximum distance between the person and the sensor is selected at a constant angle of the car seat, resulting in a measured distance of 0.98 metres.

### 6.1 Variations of both features

The first threshold optimisations are based on X and Y combinations proposed by Mr. Pech. Due to illness, the measurements were carried out without Mr. Kotzian. To get a first impression of the effects of the threshold change, Mr. Abdul and Mr. Biermann wear both only one T-shirt and sit normally in the car as can be seen in *Figure 63* and *Figure 64*. For each threshold combination, 170 FFT signals are recorded, 80 with a person and 90 with an empty seat, and the classes are stored. The following figure shows the result:

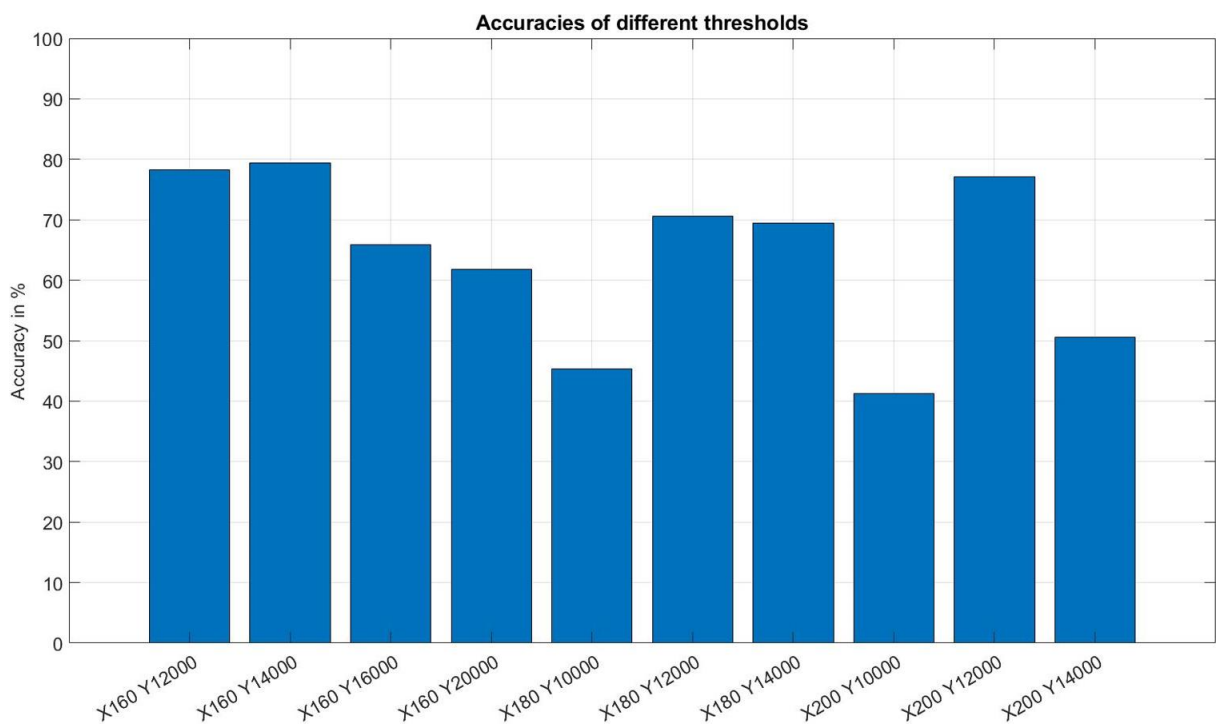


*Figure 6: Accuracies of the first threshold measurements*

The confusion matrices of the individual threshold combinations are shown in the appendix from *Figure 65* to *Figure 74*. *Figure 6* clearly shows that thresholds with a Y value of 12000 or 14000 lead to higher accuracies regardless of the X value. Compared to the accuracy of the first data set, an increase of 10.15% can be achieved with thresholds X160 and Y14000.

In an additional measurement, further threshold combinations are examined with the help of the so-called demo mode. The demo mode is used to view the results of the classes calculated by the sensor without saving the data. In this way, first tendencies towards good thresholds can be recognised with the help of human perception. This observation shows that, visually, the best classification result lies with the thresholds X140 and Y12000. To confirm the latter investigation, all group members are included in the measurements this time. The corresponding pictures of the measurements can be seen from *Figure 75* to *Figure 77* in the appendix. In addition, unlike before, 600 FFT spectra are evaluated for one threshold combination, 300 of which are related to a person in a car and 300 with an empty seat. This makes the results much more meaningful. The distance from the person in the car to the sensor as well as the angle of the seat remains the same. To check whether the thresholds X140 and Y12000 lead to the highest accuracy, further comparative measurements are taken with X and Y values close to the optically best configuration. The result of this investigation can be seen in the following figure:

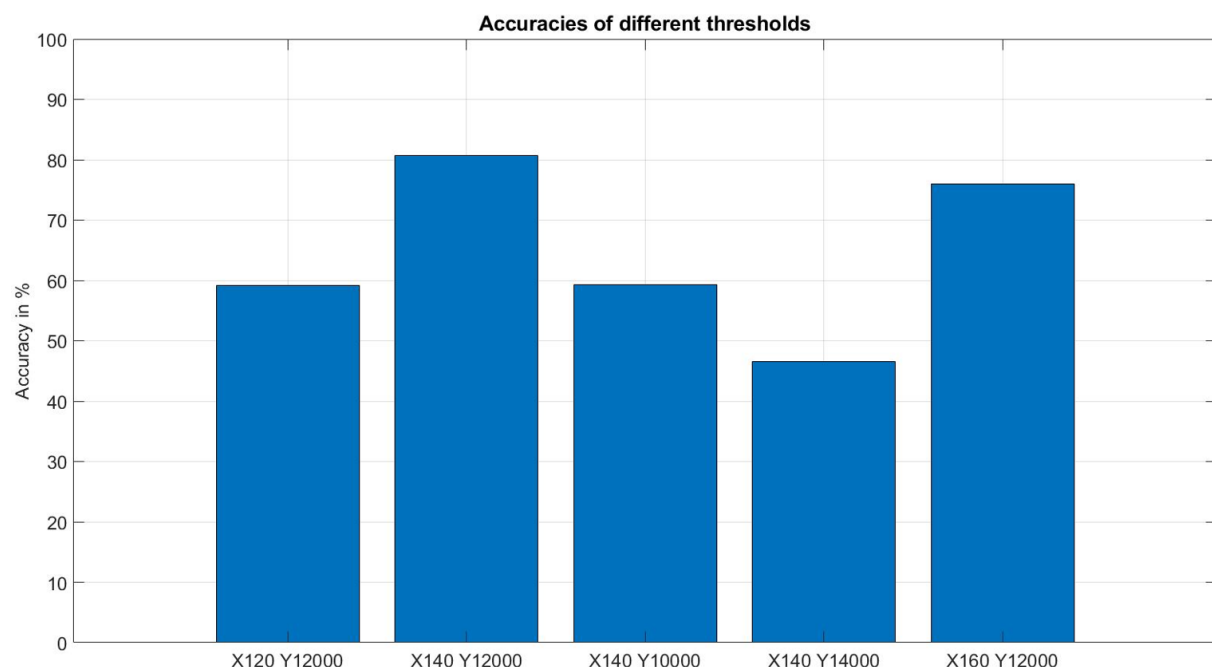


*Figure 7: Accuracies of the second threshold measurements*

In the appendix of *Figure 78* to *Figure 81* the respective confusion matrices are shown. The chart shows that the highest accuracies can be achieved with the threshold values X140 and Y12000. The resulting confusion matrix can be seen in the next figure:

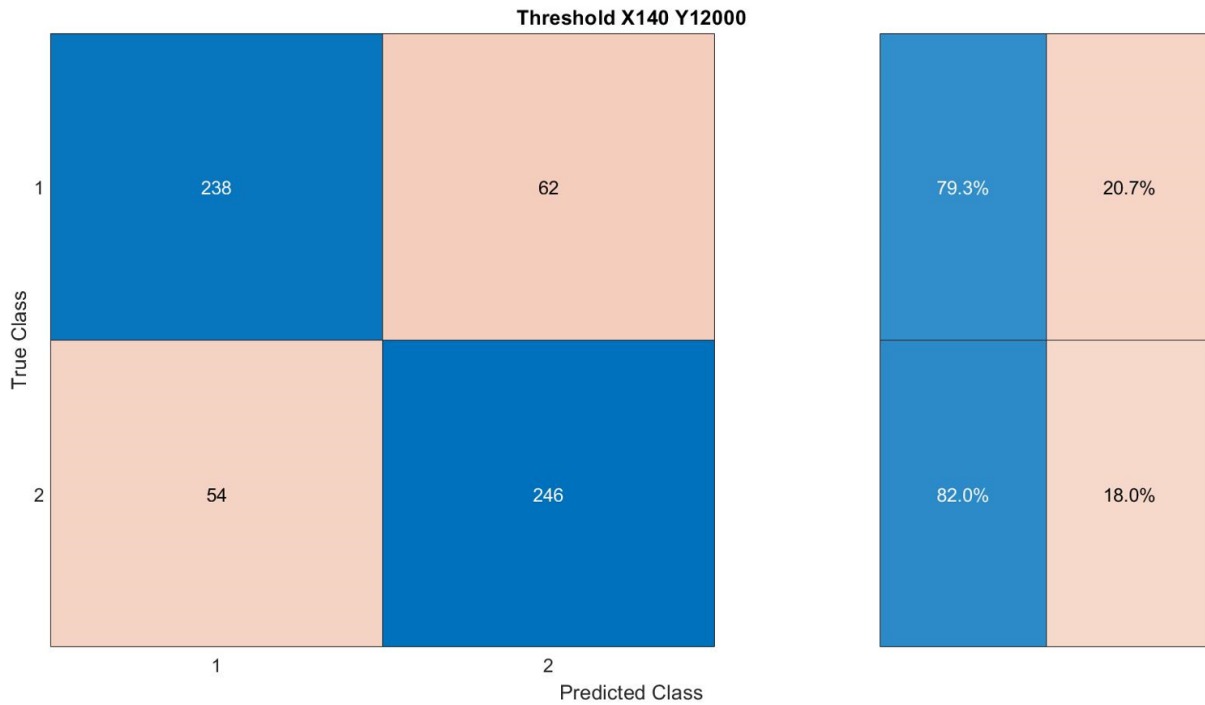


*Figure 8: Confusion matrix of thresholds X140 Y12000*

On the left side of the figure, the absolute values of correctly and incorrectly predicted classes can be seen. On the right side the so-called True Positive Rates (left blue column) and the False Negative Rates (right red column) in relation to the two classes are shown. Compared to the accuracies from the first data set, higher accuracies of the two classes can be achieved in percentage terms with these X and Y values. However, this can initially only be related to the total of 600 measurements.

## 6.2 Variations of X value (Constant Y value)

After consultation with Mr. Pech, the effect of a fixed Y value of 1000 with varying X values on the measurements is to be checked. It will also be investigated whether a further improvement in accuracy can be achieved with other threshold combinations. In addition, the event "Normal Sitting" serves as a reference for these measurements as well as the wearing of one t-shirt for each as with the threshold measurements cf. *Figure 7*. To increase the significance, 500 measurements are taken per person, resulting in 1500 measurements for the empty seat, in order to have an evenly distributed data set. The starting point for the X value is 10 and is increased step by step, i.e. in steps of 20, up to 210. The confusion matrices depending on the

different X values can be found in the appendix from *Figure 82* to *Figure 93*. The following graph shows the accuracies:

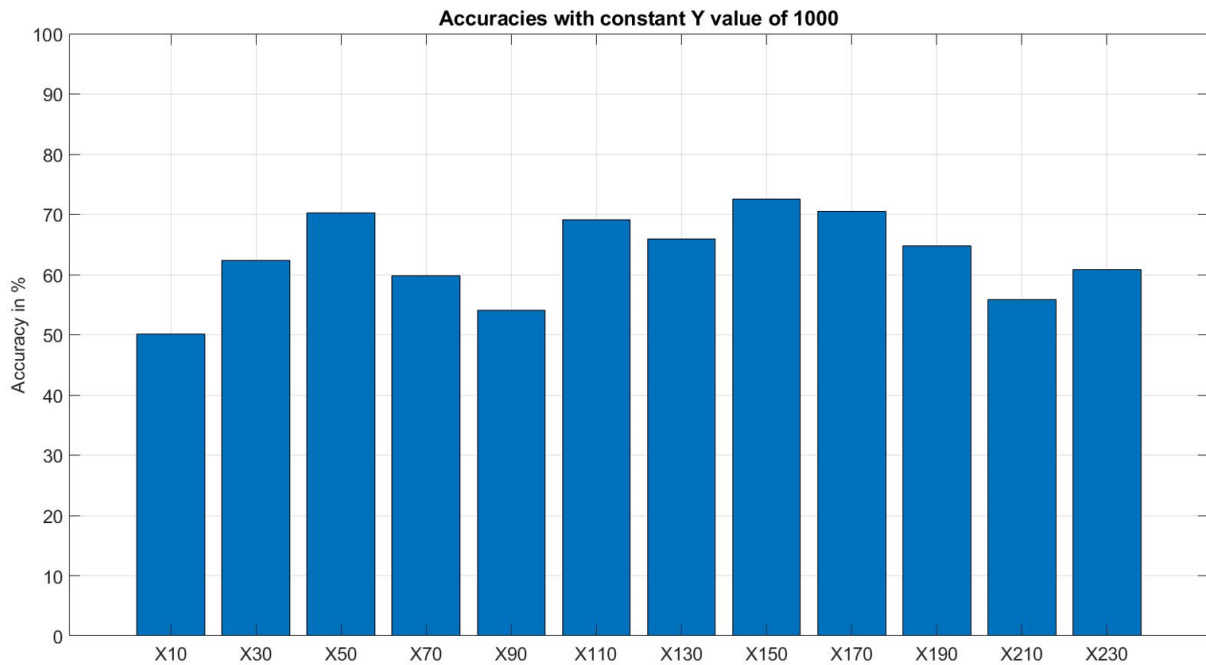


*Figure 9: Accuracies of the third threshold measurements*

Compared to the previous accuracies, no improvement in the recognition rate can be achieved with any X-Y combination. For this reason, the threshold combination X140-Y12000 as described in section 6.1 is chosen for the second data set. It is necessary to check to what extent the recognition rates change in relation to a higher number of measurements per class.

## 7 Evaluation of 2<sup>nd</sup> data set

In this chapter the second data set is evaluated, which is based on the same boundary conditions as the first data set. As described in the last chapter, the highest accuracy related to a small data set can be achieved with the thresholds X140 and Y12000. In dataset 2 we will now investigate whether the detection rates can also be transferred to a dataset with 42.000 measurements. The next figure shows the confusion matrix of the second data set:

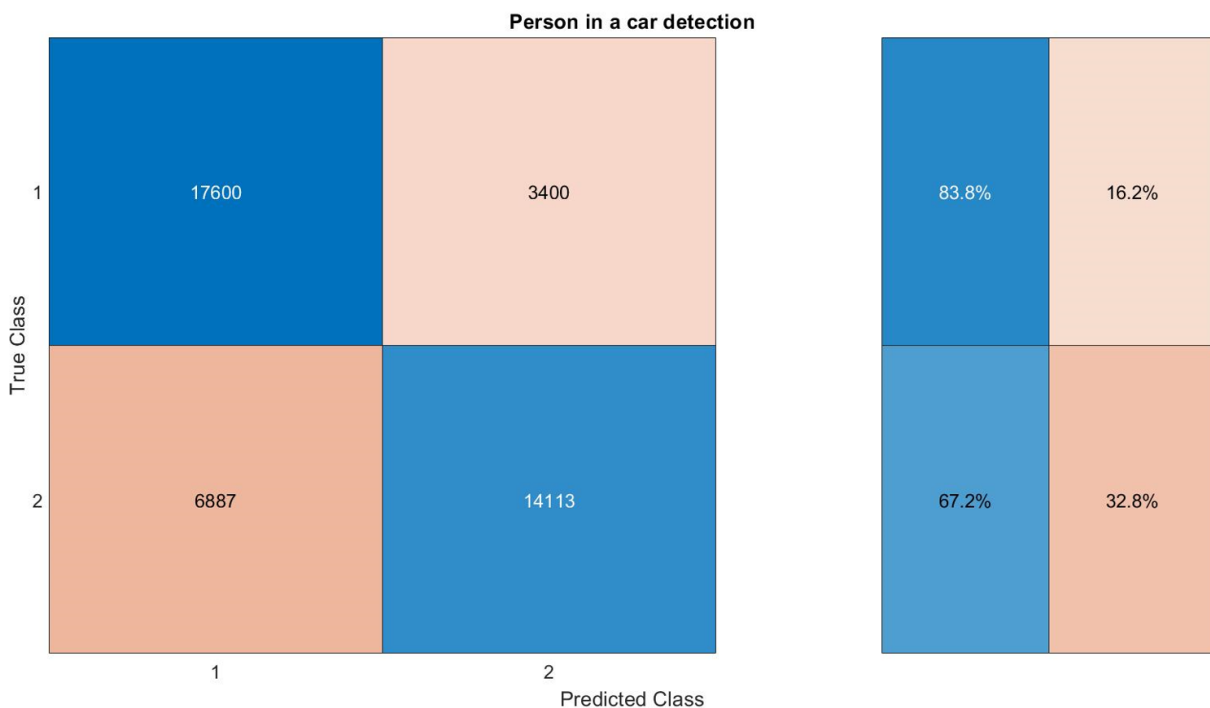
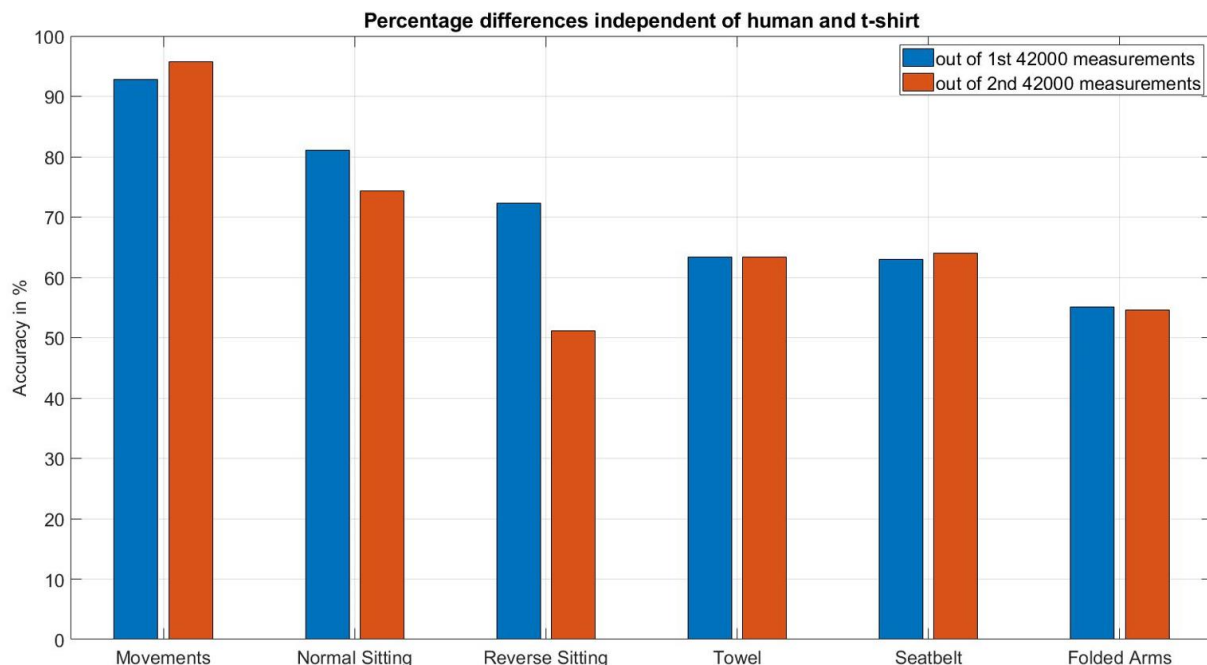


Figure 10: Confusionmatrix, TPR and FNR of the second data set

Compared with the evaluation of the confusion matrix according to *Figure 8*, it can be seen that class 1 was recognised slightly better in percentage terms, but class two was recognised around 15 percent worse. One reason for this could be that there are too few measurements for the two classes in the threshold adjustments. If further thresholds are to be adjusted in this project in the future, more measurements must be taken here in percentage terms in order to create a meaningful basis for a large data set of 42.000 measurements. Another reason for the different performance of the two classes could be an inconsistent experimental set-up, which could have been caused by the different tasks of the other groups. Inconstant in this case means a displacement of the sensor, which causes the ultrasound signals to be reflected differently and the detection rates of the classes to have a certain deviation as shown above.

Nevertheless, compared to the confusion matrix of the first data set, the threshold change results in an overall higher detection rate. Despite a slightly worse recognition rate of the second class, an empty seat can be recognised better in percentage terms. With the help of the next figure, an investigation into the reasons for the different accuracies of the second data set compared to the first data set can be found. The focus is placed on the six different events that are compared independently of the person and the t-shirt worn:



*Figure 11: Comparison of the events of the first and second data set*

The accuracies shown in blue can also be taken from *Figure 5*. It can be clearly seen that the reason for the poorer accuracy of the second class is mainly due to the event "Reverse Sitting". This is due to the fact that the latter event is the most difficult to reproduce. In addition, the ultrasonic signal is more likely to be reflected by the trousers in this event, which means that different reflections and distances can occur. Furthermore, the people wore the same t-shirts but different trousers during the measurements. This is another point for the poor reproducibility of this event. In the appendix from *Figure 94* to *Figure 97*, further comparisons between the two data sets can be found, in which the deviations related to the t-shirt worn and the event of the respective persons can be seen.

## 8 Variation of seat position

In this chapter, different lateral as well as horizontal seating positions are examined with regard to the evaluation of the accuracies for the two classes. This results in different angles of incidence of the ultrasonic signal as well as distances between the sensor and the person. Due to illness, these measurements could not be carried out with Mr Abdul. In order to nevertheless obtain meaningful results, 500 FFT spectra are recorded from each of the other two group members and the classification of the classes is recorded. The persons always wear the same t-shirt. In order to achieve an evenly distributed data set, 1000 measurements are carried out for the first class. Unlike the previous measurements, this study includes the upper sensor as well as the lower sensor. The analysis is based on two different horizontal positions and three different lateral positions. The following tables list the positions including their meanings:

*Table 5: Horizontal states*

<i>State (horizontal)</i>	<i>Description</i>	<i>Abbreviation</i>
Seat position back	Max. horizontal distance between seat and sensor	SPB
Seat position front	Min. horizontal distance between seat and sensor	SPF

*Table 6: Lateral states*

<i>State (lateral)</i>	<i>Description</i>	<i>Abbreviation</i>
Seat back	Backrest on the rear bench & angle greater than 90 degrees	SB
Seat normal	Backrest straight & angle approx. 90 degrees	SN
Seat front	Backrest turned forwards & angle smaller than 90 degrees	SF

From these horizontal and lateral positions, a total of six different states are formed. These are shown in the following illustration as examples and not to scale:

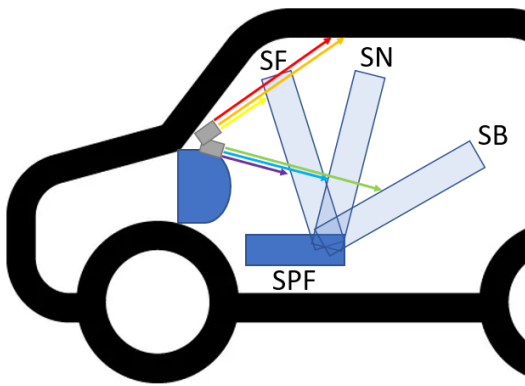


**Figure 12:** States, angles and distances for seat position front

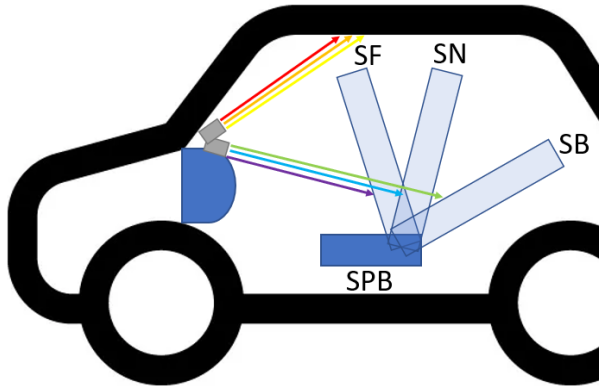


**Figure 13:** States, angles and distances for seat position front

The appendix from *Figure 98* to *Figure 115* shows the individual conditions of the measurements at the university for the empty seat and with the two test subjects. In the upper two figures, the different angles of incidence of the two sensors as well as the different distances between the positions can be seen with the help of coloured arrows. For the measurements, the distances are documented when the seat is empty and when both people are sitting in the car and the classification results of the sensors are stored. The results can be seen in the following two tables. Sensor 1 refers to the lower sensor and sensor 2 to the upper sensor:

**Table 7:** Seat position evaluation sensor 1

<i>State (Sensor 1)</i>	<i>Distance (empty seat) [m]</i>	<i>Distance (with person) [m]</i>	<i>Accuracy [%]</i>
SPF SF	0.65	differ between 0.43-0.54	0.61
SPF SN	$0.78 \pm 0.01$	$0.6 \pm 0.1$	0.72
SPF SB	$0.87 \pm 0.01$	differ between 0.98-2.35	0.86
SPB SF	$0.87 \pm 0.01$	differ between 0.65-0.89	0.86
SPB SN	$0.97 \pm 0.01$	$0.8 \pm 0.1$	0.84
SPB SB	$2.32 \pm 0.1$	differ between 1.8-2.3	0.69

**Table 8:** Seat position evaluation sensor 2

<i>State (Sensor 2)</i>	<i>Distance (empty seat) [m]</i>	<i>Distance (with person) [m]</i>	<i>Accuracy [%]</i>
SPF SF	1.26±0.01	differ between 0.38-2.25	0.7
SPF SN	differ between 0.85-1.17	differ between 0.69-2.65	0.75
SPF SB	differ between 1.07-1.16	differ between 1.04-1.16	0.3
SPB SF	1.16	differ between 0.66-2.15	0.39
SPB SN	1.05±0.01	differ between 0.9-1.15	0.68
SPB SB	1.16	1.16	0.47

For each state, the confusion matrices are shown in detail in the appendix from *Figure 116* to *Figure 127*. With sensor 1, the person is in the radar beam in every condition, which is why the accuracies are more stable. The evaluations of sensor 1 also show that the favoured thresholds with X140 and Y12000 also show good accuracies at other positions. Furthermore, with the help of the table, a conclusion can be drawn regarding an optimal distance range between sensor and person. This is approx. 0.87 metres with an empty seat and the accuracies slowly decreases in positive and negative directions. On the one hand, this is due to the selected thresholds that were evaluated close at the above-mentioned distance and on the other hand to different body parts from which the ultrasonic signal of the sensor is reflected. This is due to different angles of incidence.

The evaluation of the second sensor must be considered differently, as here the person is not in the radar beam for every condition. In the states SPF SB, SPB SF and SPB SB, the accuracies are the lowest, from which it can be deduced that the person is not sitting in the radar beam. Therefore, only the detection of the 1st class has to be considered for these states, which, however, is clearly worse for the states SPF SB and SPB SF than for SPB SB as can be seen in the confusion matrices in the appendix (*Figure 124*, *Figure 125* and *Figure 127*). This could be due to the fact that the person in the SPF SB and SPB SF states sits closer to the radar beam of the sensor and thus possibly causes slight interfering signals, e.g. through talking or movements, which then pick up the reflected signal. Nevertheless, the other accuracies are relatively high, although in these conditions it is mainly the person's face that reflects the ultrasonic signal instead of the t-shirt. However, this also shows that the favoured thresholds can be transferred to other parts of the body.

What is striking about both sensors is the fact that the distances vary more when a person is sitting in the car. This can be explained by the breathing, the body temperature and the shape of the person as well as the different t-shirts worn.

## 9 Evaluation of different objects

This chapter analyses the influence of different objects with regard to the reflected ultrasonic signal. As in the two previous data sets, the maximum horizontal distance between seat and sensor and a distance of 0.98 metres from sensor to backrest are selected. The measurements are again based only on the lower sensor. The favourite thresholds of X140 and X1200 are also set here in the GUI. The requirement described in the task to place a human-like dummy in the car is replaced by the positioning of a plastic baby on the car seat. In addition, the accuracy of other objects such as two different backpacks, an empty cardboard box and traffic cones is evaluated. The corresponding pictures of the experimental set-up at the university can be seen in the approach from *Figure 128* to *Figure 132*. The analysis is based on 500 measurements per event. The results are shown in the following figure:

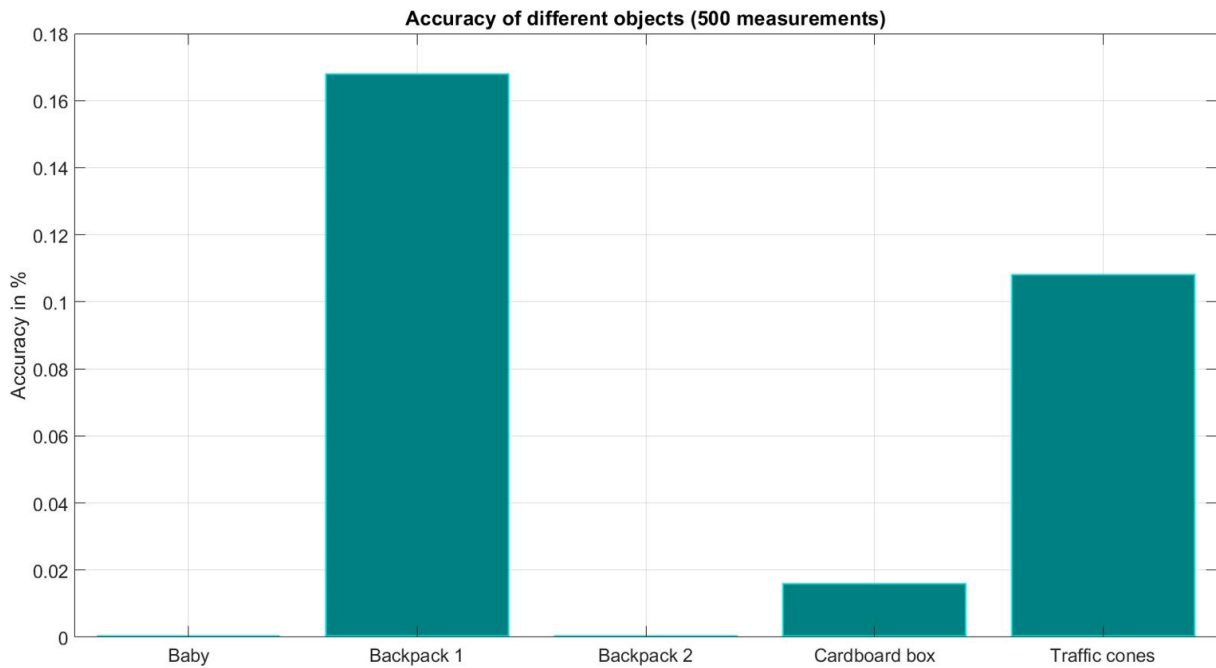


*Figure 14: Accuracy of different objects*

The main reason for the different accuracies is the reflection cross-section of an object, which is represented by the symbol sigma. A human being has a reflection cross-section of 1 and in general the latter can be determined with the following formula:

$$\sigma = 4\pi x^2 \frac{P_r}{P_t} \quad (9.1)$$

$P_r$  is the power reflected by the object, which is calculated as follows:

$$P_r = I_t R A_0 \quad (9.2)$$

The factor  $I_t$  describes the intensity transmitted to the object with the assumption that the wave front propagates as a spherical surface and depends on the emitted power of the ultrasound probe:

$$I_t = \frac{P_t}{4\pi x^2} \quad (9.3)$$

The factor  $R$  from formula 9.2 is a measure for the reflectivity of an object and the symbol  $A_0$  stands for the area of the object hit with the ultrasonic signal [24]. Together with the distance  $x$  between sensor and object, the latter factors are the main reason for the low accuracies. The plastic baby and the two backpacks have a very small  $A_0$  area due to their shape, and the cardboard box and traffic cones have a low reflectivity due to their materials. When looking at the distances between the sensor and the objects, it is noticeable that all objects except for the cardboard box are almost in the distance range optimally adjusted by the thresholds. This leads to the conclusion that the surface area and the reflectivity of the objects have the greatest influence. The distances are listed in the following table:

*Table 9: Distances of different objects*

<i>Object</i>	<i>Distance to sensor [m]</i>
Plastic baby	0.91
Traffic cones	differ between 0.82-0.85
Backpack 1	0.82
Backpack 2	0.75
Cardboard box	0.47

## 10 Machine Learning Classification

This chapter is about creating and implementing a machine learning model in Matlab. The basis for the model is the second data set with 42.000 measurements, which simultaneously represents the training data set. In order to compare the classification of the university sensor with the classification of the machine learning model presented here, a test data set with 16.800 FFT spectra is created. The ratio between training and test data set is thus about 70% to 30% and is often used to train models. The 16.800 FFT spectra are composed of 200 measurements for each of the people's events and 200 times 42 measurements for an empty seat. The procedure for recording the data is the same as for the evaluation of the first and second datasets, see chapters 5 and 7. The main goal of the machine learning model is to achieve a better classification or a higher accuracy than the university's sensor. In order to achieve this goal, it is first necessary to evaluate the accuracy of the university's sensor in relation to the test data set. The next figure shows the corresponding confusion matrix:

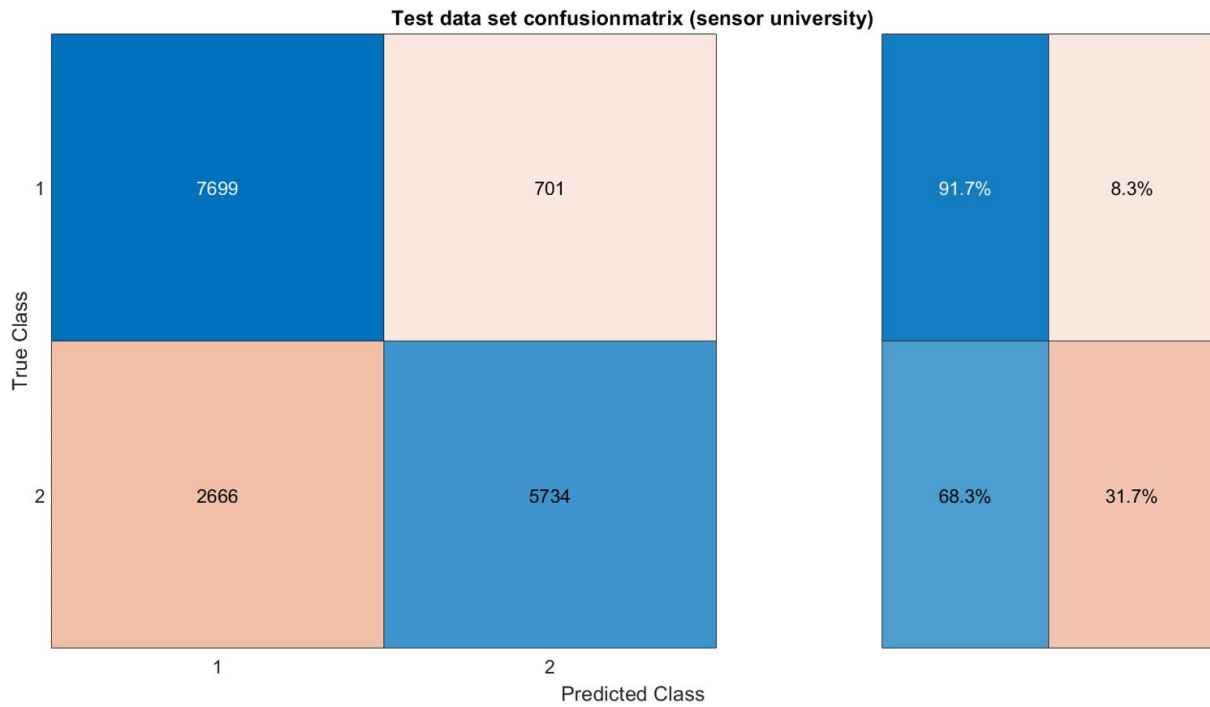


*Figure 15: Confusionmatrix of test data set (sensor classification)*

Compared to the confusion matrix of the second data set see *Figure 10*, it can be seen that the recognition of a human is significantly lower in percentage than the recognition of an empty seat. The latter is in this case even better than in the measurements of the second data set. In order to increase the recognition of a human being in particular, the machine learning model is built up step by step in the next sections. Looking back at *Figure 2*, a further step, feature selection, is inserted for this process between feature extraction and decision making.

This is to significantly increase the overall accuracy of exactly 80% of the upper confusion matrix.

## 10.1 Feature Extraction

The feature extraction follows the data acquisition/pre-processing and reduces the size of the input vectors and consequently the data set, which is implemented as the training data set in the machine learning model. The reduction of the input vectors is based on the transformation of the FFT signal, which consists of 85 data points, to a numerical output value that is supposed to be representative of the properties of the spectrum. The consideration of the x-axis representing the frequencies from 35kHz to 45kHz is purposefully neglected in this evaluation in order to test a wider range of so-called filter methods for extracting the features. The focus is placed on the y-axis, i.e. the amplitudes, which enables the evaluation of features using statistics, spectral characteristics and electromyography (EMG). The Matlab Toolbox for the EMG features can be found at [25]. The calculations and detailed explanations of all features are explained in section 4.2.

## 10.2 Feature Selection

Feature selection is about filtering out the most meaningful features to achieve the best possible pattern between the two classes. This is the last step before the data is put into different classification algorithms, i.e. this step has to be analysed in detail. The main goal here is to find features that have a high classification ability, which is associated with, for example, a low variance of consecutive data points. For this purpose, a Neighborhood Component Analysis is carried out in the following sections, which is then optimised with correlations between the features. The basis of the analysis is the training data set from which the 18 different features are extracted.

### 10.2.1 Neighborhood Component Analysis (NCA)

The Neighborhood Component Analysis is very closely related to the k-Nearest-Neighbours classification and the mathematical derivation is described in more detail in section 4.4. In Matlab there are several ways to perform this analysis. In this work, the default settings are used for various optimisation settings such as the solver, lambda or the loss function, as these

are sufficient for a general statement about the quality of the analysis. In order to achieve a non-biased comparison of the classification ability of the 18 different features, the data must be standardised beforehand (see section 4.3). In Matlab this is realised with the function `zscore()`. After standardisation, the data is entered into the analysis. The following figure shows the result:

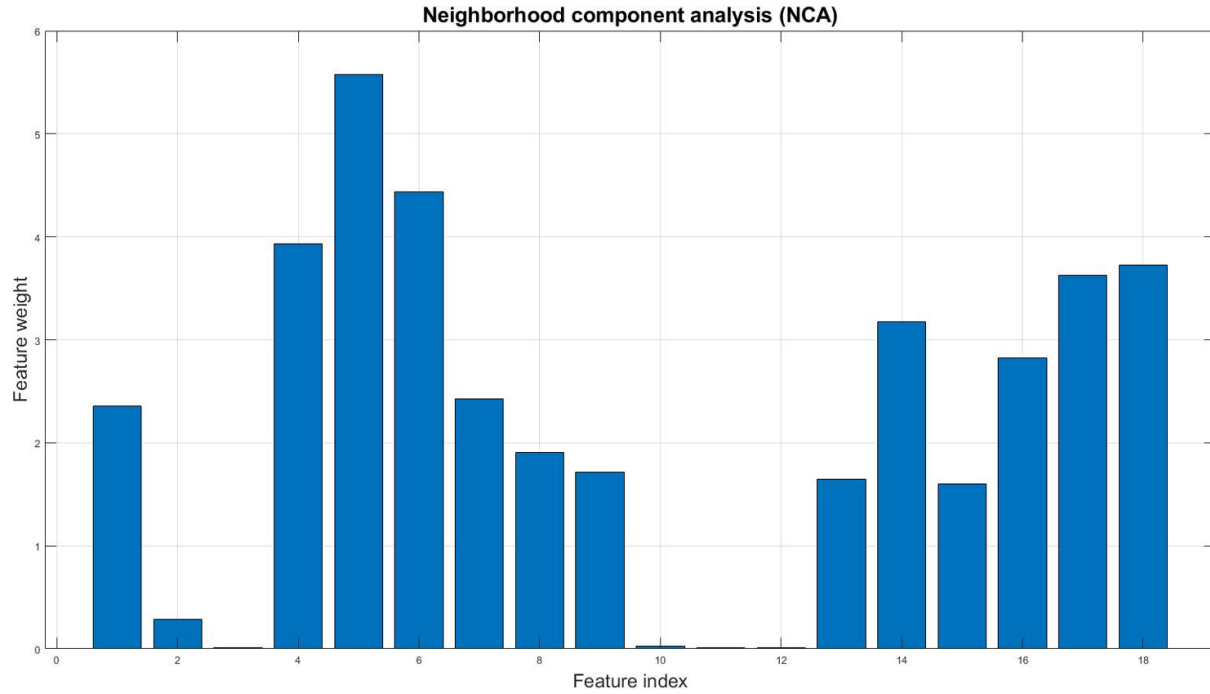


*Figure 16: Neighborhood Component Analysis of training data set*

On the x-axis, the 18 different features are listed in order of their index. The latter can be looked up in section 4.2. The y-axis describes the so-called "feature weights", which are shown with the help of bar graphs. The higher the weight of a feature, the more important it is for the implementation in a classification algorithm. The following table lists the seven highest weighted features including their index and names:

*Table 10: The seven most important features based on NCA*

Index	Feature name	Feature weight
5	Occupied bandwidth	5.62
6	Power bandwidth	4.37
4	Equivalent noise bandwidth	3.92
18	Maximum fractal length	3.78
17	Logarithmic Teager Kaiser Energy Operator	3.65
14	Skewness	3.19
16	Enhanced Wavelength	2.82

Only the seven most important features are listed, as the weighting of the following features is considered too low and the machine learning model should be kept as simple as possible. This means a model that contains the smallest possible number of features and achieves the highest possible recognition rate. In addition, it can be seen in the table that both spectral and statistics features as well as EMG features are represented. The determined weights are not taken over into the implementation of the classification algorithm, as the order can only be considered as ordinally scaled or equivalent.

### 10.2.2 Correlations

As described earlier in this chapter, correlations among the features are evaluated to optimise the Neighbourhood Component Analysis. The aim of this is to eliminate redundant features that have a higher correlation than 0.7 or a lower correlation of less than -0.7 in order to provide new information with each feature. In this way, the machine learning model can be simplified and only independent features are used to classify the two classes. The correlation matrix of the seven features can be seen in the figure below:

	Index 4	Index 5	Index 6	Index 14	Index 16	Index 17	Index 18
Index 4	1,00						
Index 5	-0,19	1,00					
Index 6	0,95	-0,16	1,00				
Index 14	0,42	0,15	0,22	1,00			
Index 16	-0,69	0,46	-0,71	-0,13	1,00		
Index 17	0,33	-0,13	0,27	0,18	-0,02	1,00	
Index 18	-0,57	0,44	-0,60	-0,02	0,91	0,20	1,00

Figure 17: Correlation matrix of the different features

Features that show a high correlation to a feature that has a higher weighting are eliminated. With this approach, the redundancy of features with indexes 4 and 16 can be avoided as they are removed from the machine learning model. This leaves five features for implementation in the classification algorithm.

### 10.3 Decision making

The features extracted and selected in the previous sections are given into different classification algorithms in this chapter. The aim is to achieve the highest possible accuracy of the test data in order to achieve a better result than the sensor at the university. The evaluation of different classification algorithms is done in the Classification Learner App in Matlab [26].

In the latter, the data can be given into various algorithms such as decision trees, Naive Bayes, KNN, SVM and neural networks. To gain an insight into the classification capability of the two most important features with the indexes 5 and 6, the following figure shows a scatter plot in which a first and simple classification of the two classes of the training data set becomes visible:

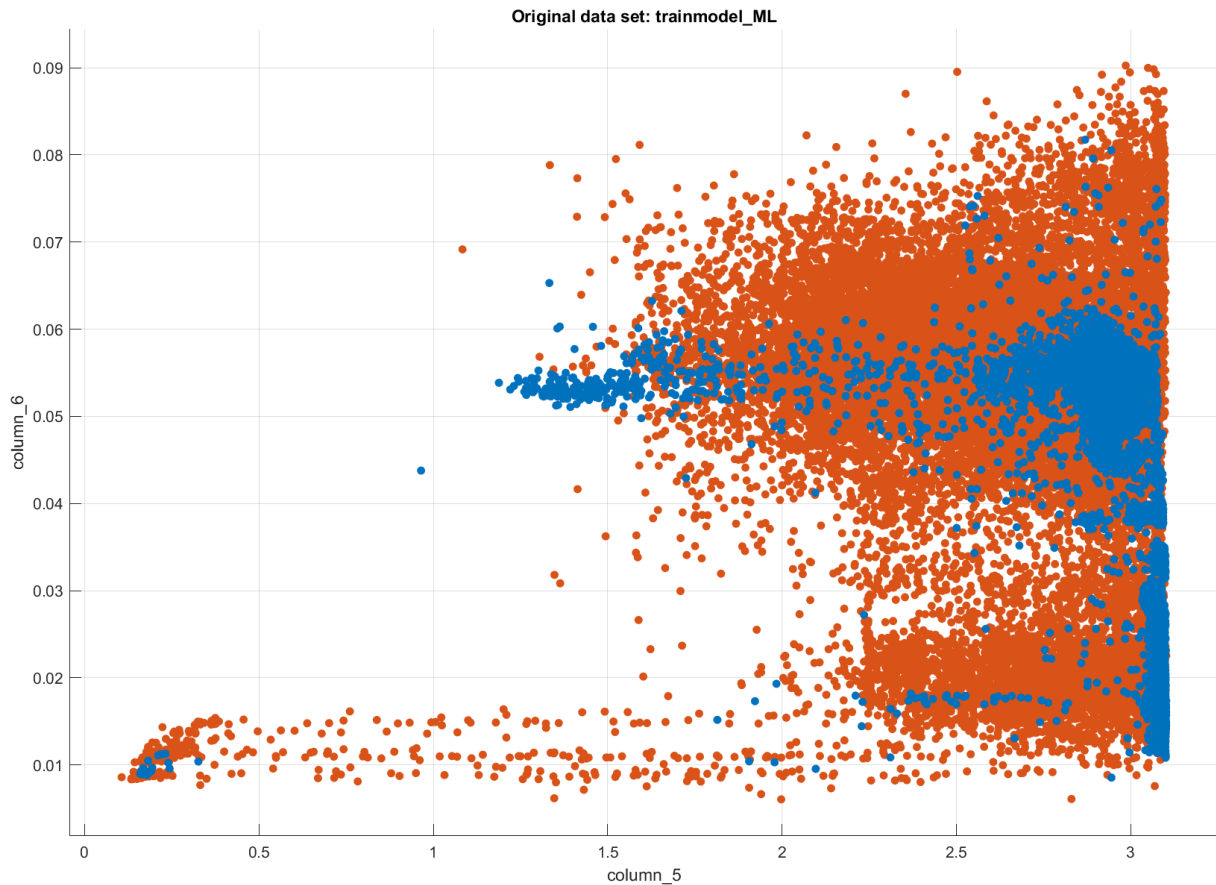


*Figure 18: Exemplary classification with the help of two features*

The colour blue represents the detection of an empty seat and the colour orange the detection of a human being regardless of its event. With the help of these two features, a good visual classification is possible.

To avoid an overfitted machine learning model, a 5-fold cross-validation is applied to the training dataset. This results in a validation accuracy that, in the best case, should roughly correspond to the test accuracy. When this is the case, we speak of a generalised model that correctly recognises the tendencies in the data and does not learn the data by heart. If the model has a high generalisation, it can then be applied to other test data sets. In addition to the generalisation, the prediction speed, the training time and the required memory space are

also included as criteria for deciding on a suitable classification algorithm. The evaluation table of the 25 different algorithms is shown in the appendix in *Table 12*. The five algorithms that achieve the best generalisation and accuracy are listed in the following table including the other criteria. The table is ordered in descending order with respect to the highest test accuracy:

*Table 11: Comparison of the five best classifiers*

Classifier	ACCVAL [%]	ACCTEST [%]	PS [ $\mu$ s/Pred.]	Tt [s]	MS [MB]
Coarse Gaussian SVM	95,2	96,1	18,52	21,66	0,83
Medium NN	97,7	95,1	0,67	98,82	0,01
Coarse KNN	96,2	94,3	14,49	3,09	5,214
Fine KNN	97,2	93,2	2,17	0,88	5,214
Weighted KNN	97,5	92,5	4,55	1,34	5,214

With regard to an implementation of the machine learning model, as in this case in an intelligent sensor, storage capacities are usually limited. Due to this fact, the model using the medium neural network classifier would be the most suitable variant, as only 0.01 megabyte of memory is required. The medium neural network is a feedforward neural network and is based on two fully connected layers with 25 neurons and a ReLU activation function in the first and with 2 neurons and a softmax activation function in the second hidden layer. Moreover, only 0.67 microseconds are required for a prediction. The training time plays a subordinate role, since the training data does not change dynamically with this classification.

If enough storage space, i.e. at least 0.83 megabyte, is available for a possible integration and the prediction speed is compatible with the output of the classes, an even higher accuracy could be achieved with the implementation of a Coarse Gaussian SVM algorithm. Its structure and mode of operation are explained in more detail in the theoretical principles under 4.5. Compared to the classification results of the sensor at the university, an increase of 16.1% can be achieved with this machine learning model in relation to the test data. This results in the following confusion matrix:

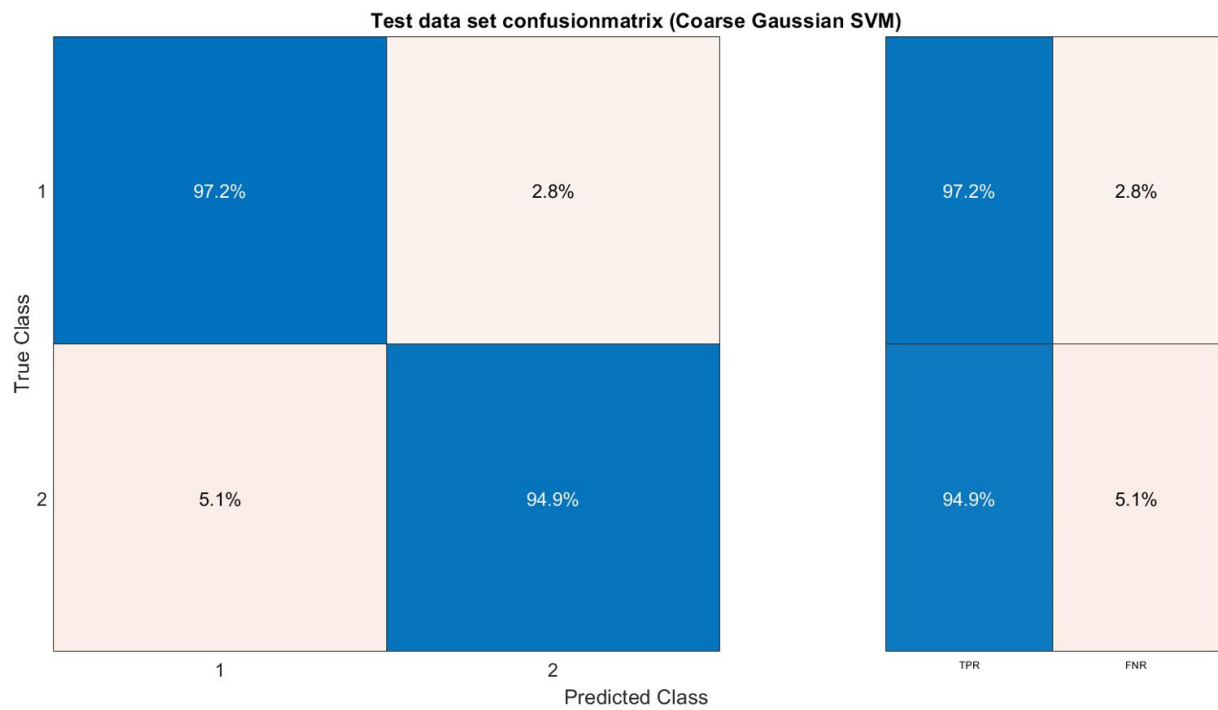


*Figure 19: Confusionmatrix of test data set (MLM classification)*

The 97.2% percent corresponds to 8164 correct detections from 8400 and the 94.9% is based on 7973 correctly detected measurements from 8400. Compared to the confusion matrix (see *Figure 15*), this machine learning model significantly increases the accuracy of detecting an empty seat by 5.5% and detecting a person with different activities by 26.6%.

## 11 Summary and outlook

The aim of this work was to perform a reliability test on an existing ultrasonic sensor system that can distinguish between an empty seat and a person in the car.

In the first step, a data set with the default values for the features number 1 and 10 was evaluated. This showed an accuracy of the two classes of about 70%. Through various threshold adjustments based on the change of the above-mentioned features, an 6.25% improvement in accuracy was achieved with the help of the threshold combination X140 and Y12000. This result is reflected in the confusion matrix of the second data set.

When the seat position was subsequently varied, it became clear that the accuracies were also high for other seat positions and that the optimal detection range was 0.87 metres between sensor 1 and the empty seat. Since the test persons do not sit in the radar beam at every position with sensor 2, it can only be used for certain seating positions.

The evaluation of different objects has shown that low accuracies occur due to low reflection cross-sections. The main influencing factors here are cross-sections that are too small and poor reflection properties of the tested objects.

In the following creation of the machine learning model, the extracted features from the areas of statistics, spectral measurements and EMG were filtered according to their importance in the feature selection using a Neighborhood Component Analysis. With the help of correlations, redundant features were eliminated, which ultimately resulted in five features in the implementation of the classification algorithm.

When choosing the classification algorithm, it was found out that the medium neural network has the lowest memory requirements and the fastest prediction speed, but the Coarse Gaussian SVM algorithm has the highest accuracy. The latter algorithm was finally selected, resulting in an improvement of 16% in the accuracy of the test data compared to the evaluation of the existing sensor system.

With regard to the integration of the machine learning model, the factors of memory requirements, recognition rate and prediction speed must be weighed up to determine which algorithm can be implemented.

## List of references

- [1] T. Li, J. Yan, Y. Cao und J. Bajo, Hg., *Intelligent Sensors for Positioning, Tracking, Monitoring, Navigation and Smart Sensing in Smart Cities*. Basel, Switzerland: MDPI - Multidisciplinary Digital Publishing Institute, 2021. [Online]. Verfügbar unter: <https://directory.doabooks.org/handle/20.500.12854/68433>
- [2] Yalung. Christofer N. und C. M. S. Adolfo, *Analysis of obstacle detection using ultrasonic sensor*, 2017. [Online]. Verfügbar unter: <https://www.semanticscholar.org/paper/Analysis-of-Obstacle-Detection-Using-Ultrasonic-Yalung-Adolfo/b68ff6e09a794c5b92273053dd6d722531da0f68>
- [3] Sonia, A. M. Tripathi, R. D. Baruah und S. B. Nair, „Ultrasonic sensor-based human detector using one-class classifiers“ in *2015 IEEE International Conference on Evolving and Adaptive Intelligent Systems (EAIS)*, 2015, doi: 10.1109/eais.2015.7368797.
- [4] T. van Groeningen, H. Driessen, J. Söhl und R. Vôute, „AN ULTRASONIC SENSOR FOR HUMAN PRESENCE DETECTION TO ASSIST RESCUE WORK IN LARGE BUILDINGS“, *ISPRS Ann. Photogramm. Remote Sens. Spatial Inf. Sci.*, IV-4/W7, 2018, doi: 10.5194/isprs-annals-IV-4-W7-135-2018.
- [5] P. Nauth, *Autonomous Intelligent Systems*. [Online]. Verfügbar unter: <https://moodle.frankfurt-university.de/course/view.php?id=9560> (Zugriff am: 9. April 2022).
- [6] P. Nauth und A. Pech, *AIS\_Project\_Sensor\_Introduction*. [Online]. Verfügbar unter: <https://moodle.frankfurt-university.de/course/view.php?id=9560> (Zugriff am: 9. April 2022).
- [7] N. Anju Latha, B. Rama Murthy, K. Bharat Kumar, *Distance sensing with ultrasonic sensor and Arduino*, 2016. [Online]. Verfügbar unter: <https://www.ijariit.com/manuscripts/v2i5/V2I5-1189.pdf>
- [8] J. Sim, S. Kim, H. J. Park und J.-H. Choi, „A Tutorial for Feature Engineering in the Prognostics and Health Management of Gears and Bearings“, *Applied Sciences*, Jg. 10, Nr. 16, 2020, doi: 10.3390/app10165639.
- [9] MathWorks, *bandpower: Band power*. [Online]. Verfügbar unter: [https://de.mathworks.com/help/signal/ref/bandpower.html?s\\_tid=doc\\_ta](https://de.mathworks.com/help/signal/ref/bandpower.html?s_tid=doc_ta) (Zugriff am: 9. April 2022).

- [10] MathWorks, *obw*: *Occupied bandwidth*. [Online]. Verfügbar unter: [https://de.mathworks.com/help/signal/ref/obw.html?s\\_tid=doc\\_ta](https://de.mathworks.com/help/signal/ref/obw.html?s_tid=doc_ta) (Zugriff am: 9. April 2022).
- [11] MathWorks, *powerbw*: *Power bandwidth*. [Online]. Verfügbar unter: [https://de.mathworks.com/help/signal/ref/powerbw.html?s\\_tid=doc\\_ta](https://de.mathworks.com/help/signal/ref/powerbw.html?s_tid=doc_ta) (Zugriff am: 9. April 2022).
- [12] MathWorks, *enbw*: *Equivalent noise bandwidth*. [Online]. Verfügbar unter: <https://de.mathworks.com/help/signal/ref/enbw.html> (Zugriff am: 9. April 2022).
- [13] RF - SNR vs SINAD. [Online]. Verfügbar unter: [http://www.sharetechnote.com/html/RF\\_Handbook\\_SNR.bak](http://www.sharetechnote.com/html/RF_Handbook_SNR.bak) (Zugriff am: 9. April 2022).
- [14] J. Too, A. Rahim und N. Mohd, „Classification of Hand Movements based on Discrete Wavelet Transform and Enhanced Feature Extraction“, *IJACSA*, Jg. 10, Nr. 6, 2019, doi: 10.14569/IJACSA.2019.0100612.
- [15] R. N. Khushaba, A. H. Al-Timemy, A. Al-Ani und A. Al-Jumaily, „A Framework of Temporal-Spatial Descriptors-Based Feature Extraction for Improved Myoelectric Pattern Recognition“ (eng), *IEEE transactions on neural systems and rehabilitation engineering : a publication of the IEEE Engineering in Medicine and Biology Society*, Jg. 25, Nr. 10, 2017, doi: 10.1109/TNSRE.2017.2687520.
- [16] A. Phinyomark, P. Phukpattaranont und C. Limsakul, „Fractal analysis features for weak and single-channel upper-limb EMG signals“, *Expert Systems with Applications*, Jg. 39, Nr. 12, S. 11156–11163, 2012, doi: 10.1016/j.eswa.2012.03.039.
- [17] A. Aylin Tokuç, *Why Feature Scaling in SVM?: SVM and Feature Scaling*. [Online]. Verfügbar unter: <https://www.baeldung.com/cs/svm-feature-scaling> (Zugriff am: 5. April 2022).
- [18] C. M. Bishop, *Pattern Recognition and Machine Learning*, 1. Aufl. New York, NY: Springer New York, 2016. [Online]. Verfügbar unter: <http://www.springer.com/>
- [19] S. Richter, *Statistisches und maschinelles Lernen: Gängige Verfahren im Überblick*, 1. Aufl. Berlin, Heidelberg: Springer Berlin Heidelberg, 2019. [Online]. Verfügbar unter: <http://nbn-resolving.org/urn:nbn:de:bsz:31-epflicht-1548208>
- [20] W. Yang, K. Wang und W. Zuo, *Neighborhood component feature selection for high-dimensional data*, 2012. [Online]. Verfügbar unter:

[https://www.researchgate.net/profile/wangmeng-zuo/publication/220405724\\_neighborhood\\_component\\_feature\\_selection\\_for\\_high-dimensional\\_data/links/0912f51107d6a2c931000000/neighborhood-component-feature-selection-for-high-dimensional-data.pdf](https://www.researchgate.net/profile/wangmeng-zuo/publication/220405724_neighborhood_component_feature_selection_for_high-dimensional_data/links/0912f51107d6a2c931000000/neighborhood-component-feature-selection-for-high-dimensional-data.pdf)

- [21] B. S. Bhati und C. S. Rai, „Intrusion detection technique using Coarse Gaussian SVM“, *IJGUC*, Jg. 12, Nr. 1, 2021, Art. no. 112458, doi: 10.1504/IJGUC.2021.112458.
- [22] C. Savas und F. Dovis, „The Impact of Different Kernel Functions on the Performance of Scintillation Detection Based on Support Vector Machines“ (eng), *Sensors (Basel, Switzerland)*, Jg. 19, Nr. 23, 2019, doi: 10.3390/s19235219.
- [23] MathWorks, *fitcsvm: Train support vector machine (SVM) classifier for one-class and binary classification*. More about. [Online]. Verfügbar unter:  
<https://de.mathworks.com/help/stats/fitcsvm.html#bt7oo83-5> (Zugriff am: 2. April 2022).
- [24] P. Nauth, *Intelligent Sensors* (Zugriff am: 9. April 2022).
- [25] Jingwei Too, *EMG Feature Extraction Toolbox*. [Online]. Verfügbar unter:  
<https://de.mathworks.com/matlabcentral/fileexchange/71514-emg-feature-extraction-toolbox> (Zugriff am: 16. April 2022).
- [26] MathWorks, *Classification Learner: Train models to classify data using supervised machine learning*. [Online]. Verfügbar unter:  
<https://de.mathworks.com/help/stats/classificationlearner-app.html> (Zugriff am: 8. April 2022).

## Appendix



**Figure 20:** Measurement with no passenger



**Figure 21:** Normal Sitting RT Saboor



**Figure 22:** Reverse Sitting RT Saboor



**Figure 23:** Seatbelt RT Saboor



**Figure 24:** Movements RT Saboor



**Figure 25:** Folded arms RT Saboor



**Figure 26:** Towel RT Saboor



**Figure 27:** Normal Sitting GT Saboor



**Figure 28:** Reverse Sitting GT Saboor



**Figure 29:** Seatbelt GT Saboor



**Figure 30:** Movements GT Saboor



**Figure 31:** Folded arms GT Saboor



*Figure 32: Towel GT Saboor*

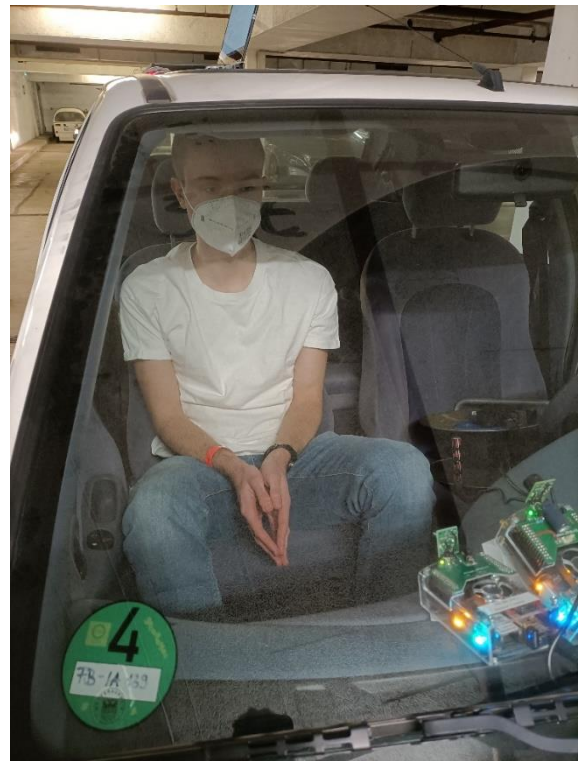


*Figure 33: Normal Sitting JWT Tobias*



*Figure 34: Reverse Sitting JWT Tobias*



*Figure 35: Seatbelt JWT Tobias*



*Figure 36: Movements JWT Tobias*



*Figure 37: Folded arms JWT Tobias*



*Figure 38: Towel JWT Tobias*



*Figure 39: Normal Sitting BT Tobias*



*Figure 40: Reverse Sitting BT Tobias*



*Figure 41: Seatbelt BT Tobias*



*Figure 42: Movements BT Tobias*



*Figure 43: Folded arms BT Tobias*



Figure 44: Towel BT Tobias



Figure 45: Normal Sitting WT Tobias



Figure 46: Reverse Sitting WT Tobias



Figure 47: Seatbelt WT Tobias



*Figure 48: Movements WT Tobias*



*Figure 49: Folded arms WT Tobias*

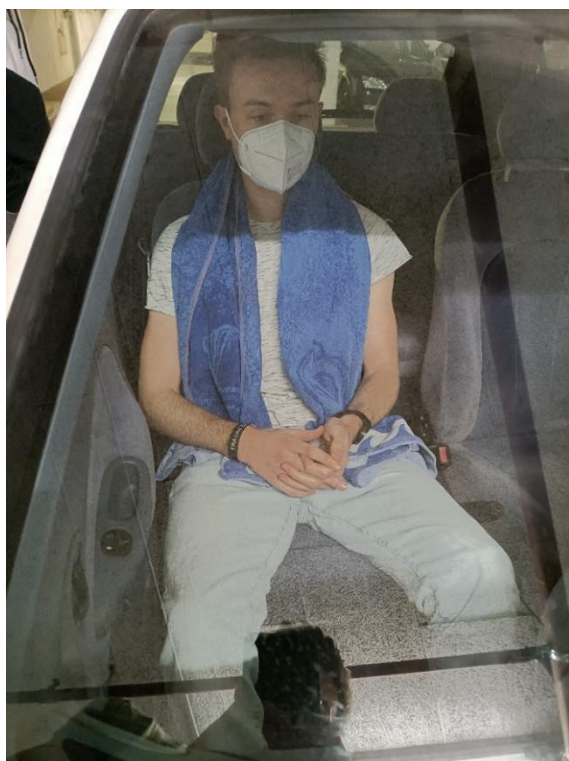


*Figure 50: Towel WT Tobias*



*Figure 51: Normal Sitting TT Tobias*



**Figure 52:** Reverse Sitting TT Tobias



**Figure 53:** Seatbelt TT Tobias



**Figure 54:** Movements TT Tobias



**Figure 55:** Folded arms TT Tobias



*Figure 56: Towel TT Tobias*



*Figure 57: Normal Sitting GT Sascha*



*Figure 58: Reverse Sitting GT Sascha*



*Figure 59: Seatbelt GT Sascha*



*Figure 60: Movements GT Sascha*



*Figure 61: Folded arms GT Sascha*



*Figure 62: Towel GT Sascha*



**Figure 63:** Threshold Measurement 1 Saboor



**Figure 64:** Threshold Measurement 1 Tobias

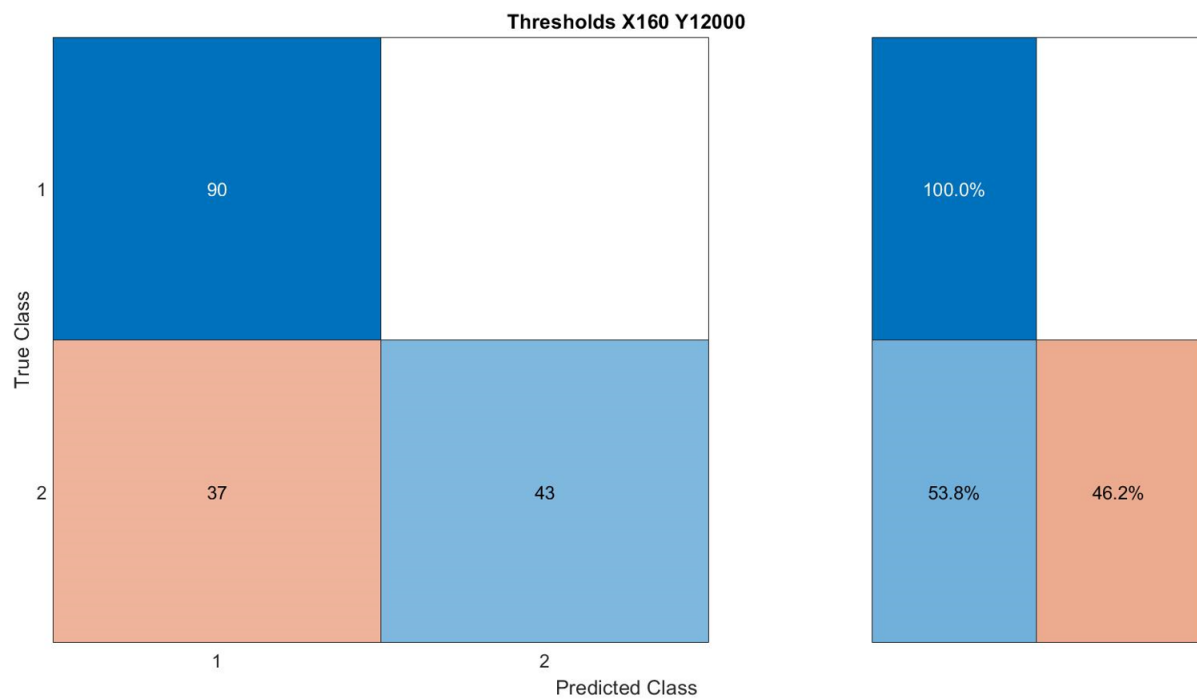


**Figure 65:** Confusion matrix of thresholds X160 Y12000

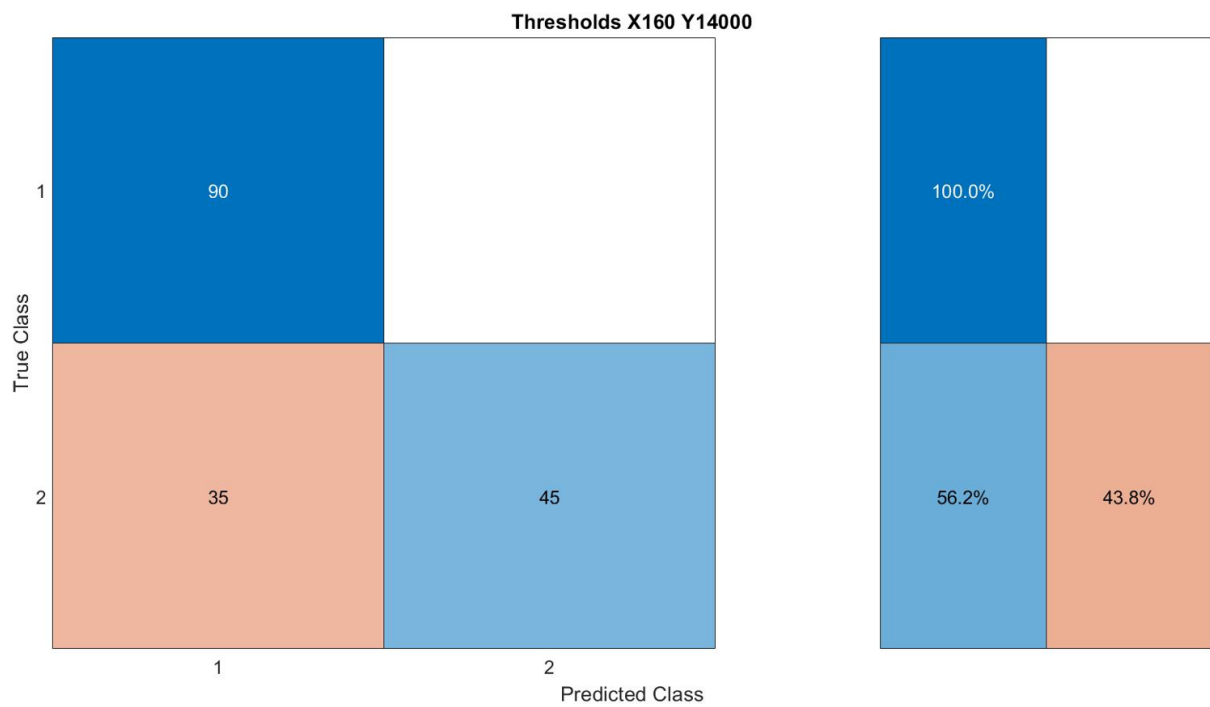


*Figure 66: Confusion matrix of thresholds X160 Y14000*

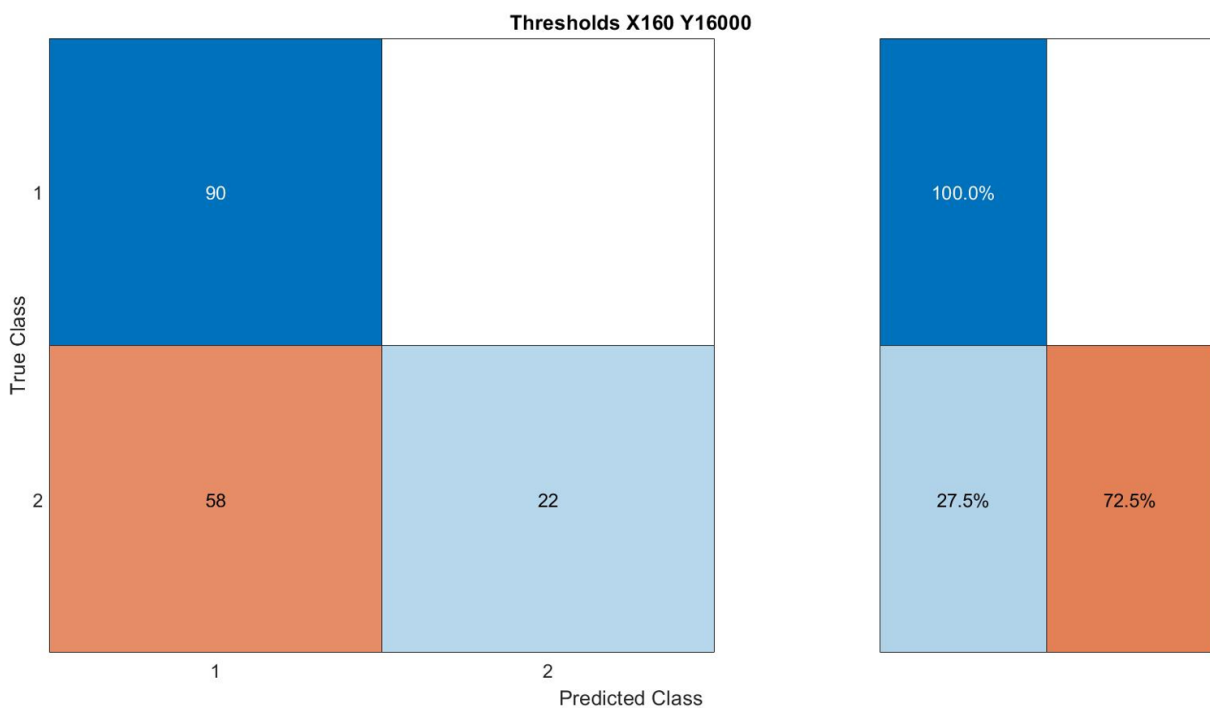


*Figure 67: Confusion matrix of thresholds X160 Y16000*

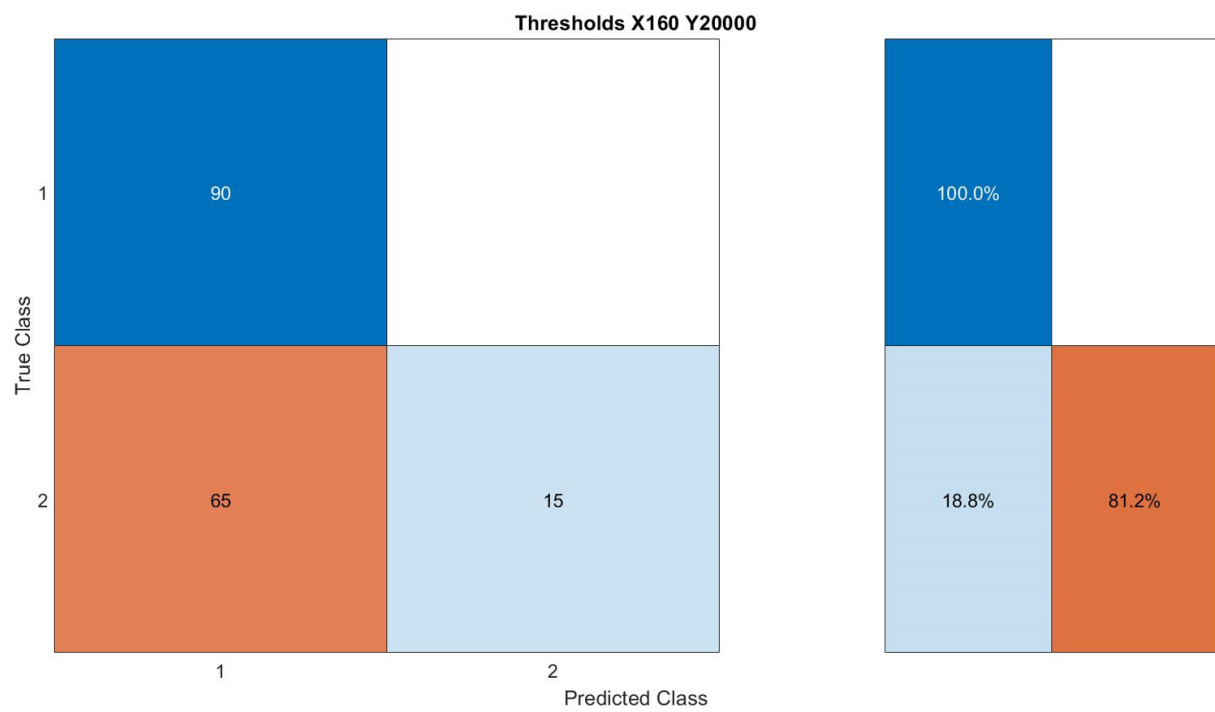


*Figure 68:* Confusion matrix of thresholds X160 Y20000

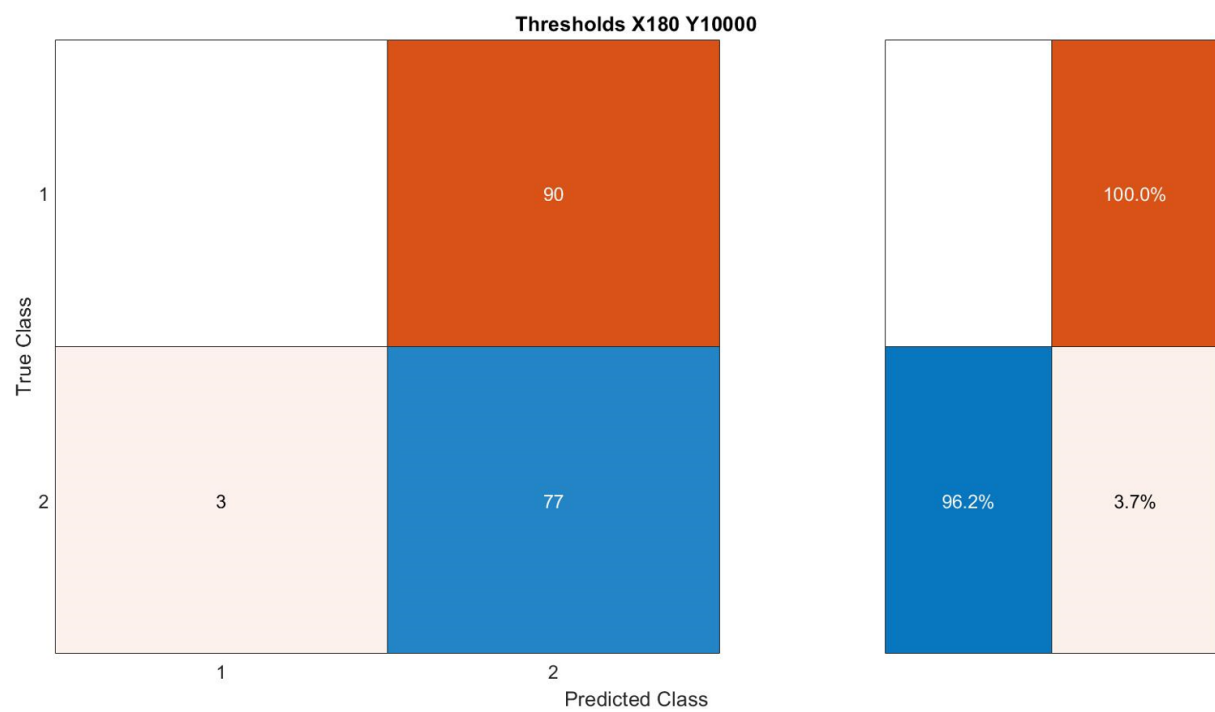


*Figure 69:* Confusion matrix of thresholds X180 Y10000

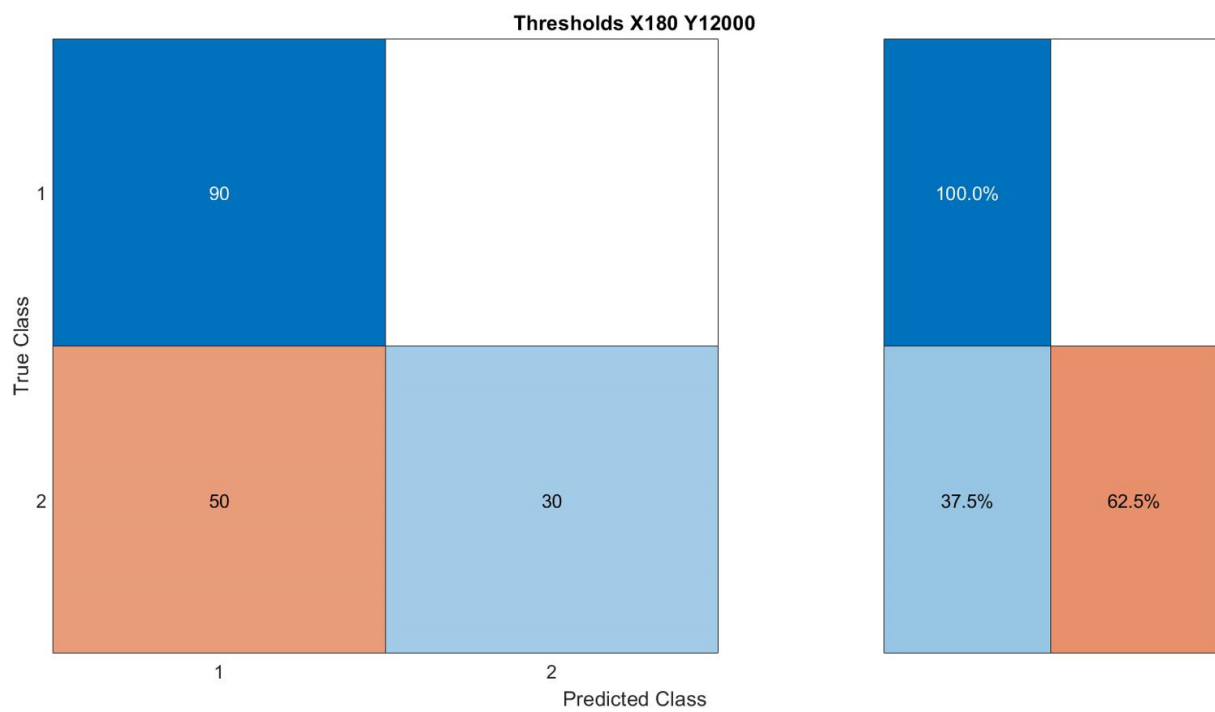


*Figure 70:* Confusion matrix of thresholds X180 Y12000

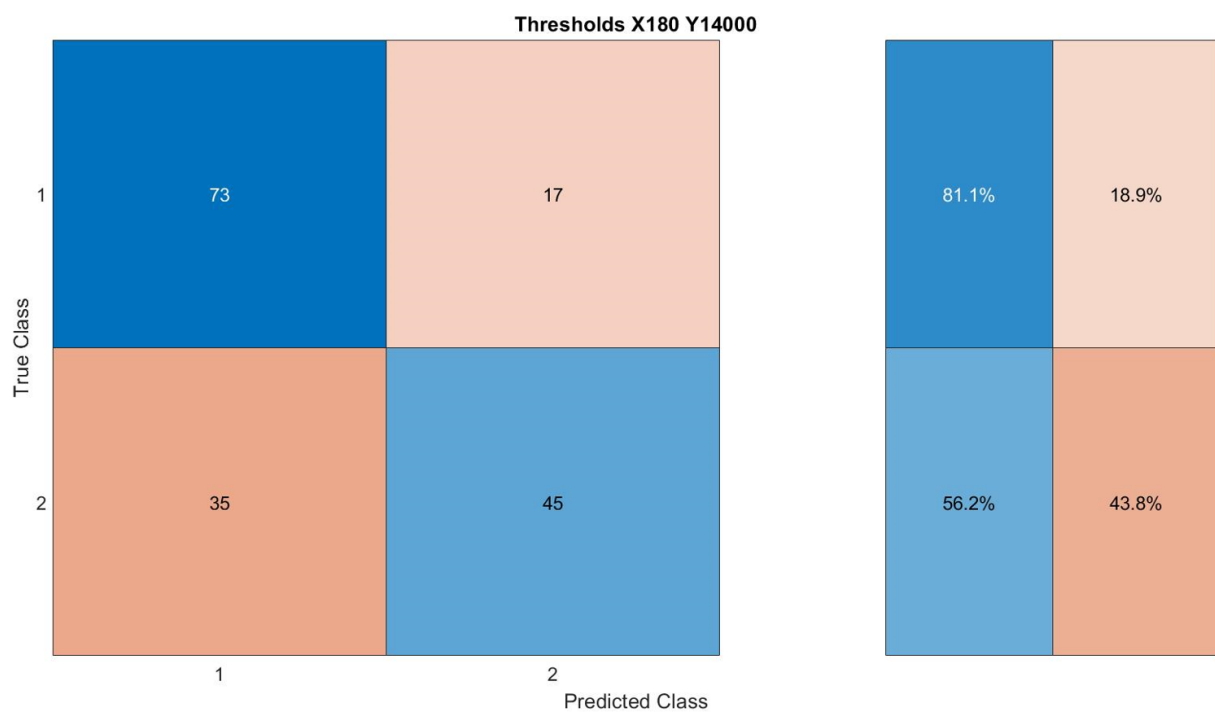


*Figure 71:* Confusion matrix of thresholds X180 Y14000

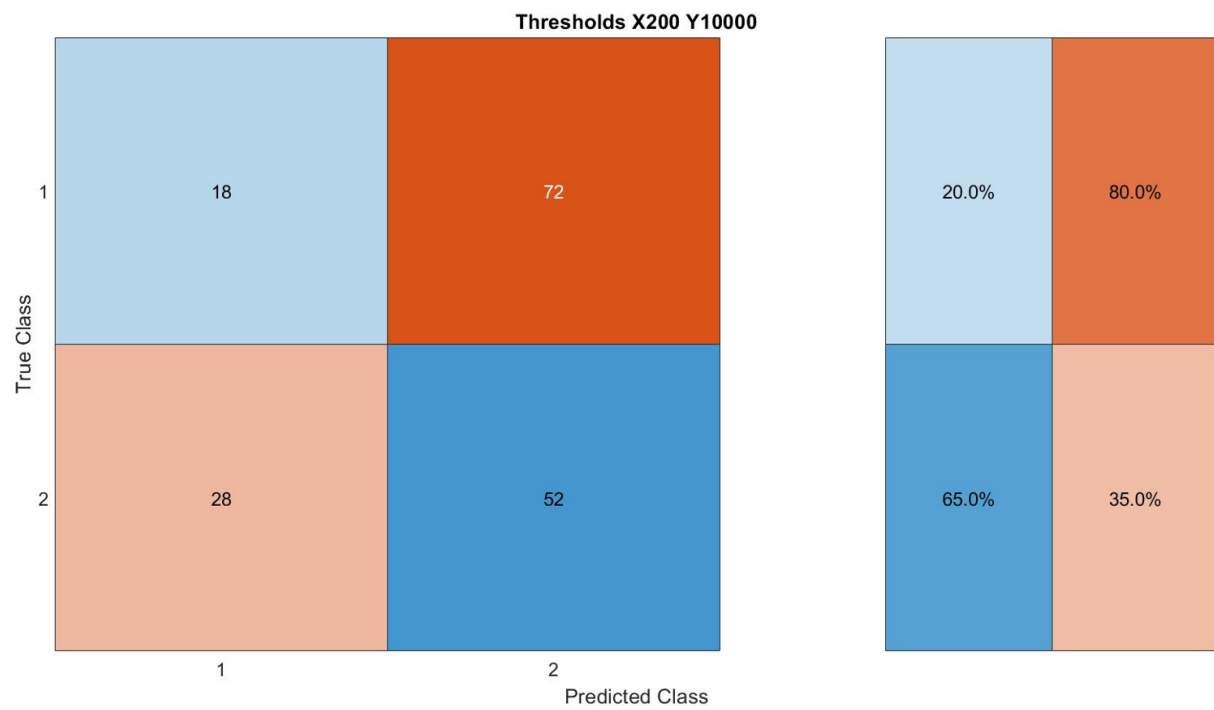


*Figure 72: Confusion matrix of thresholds X200 Y10000*

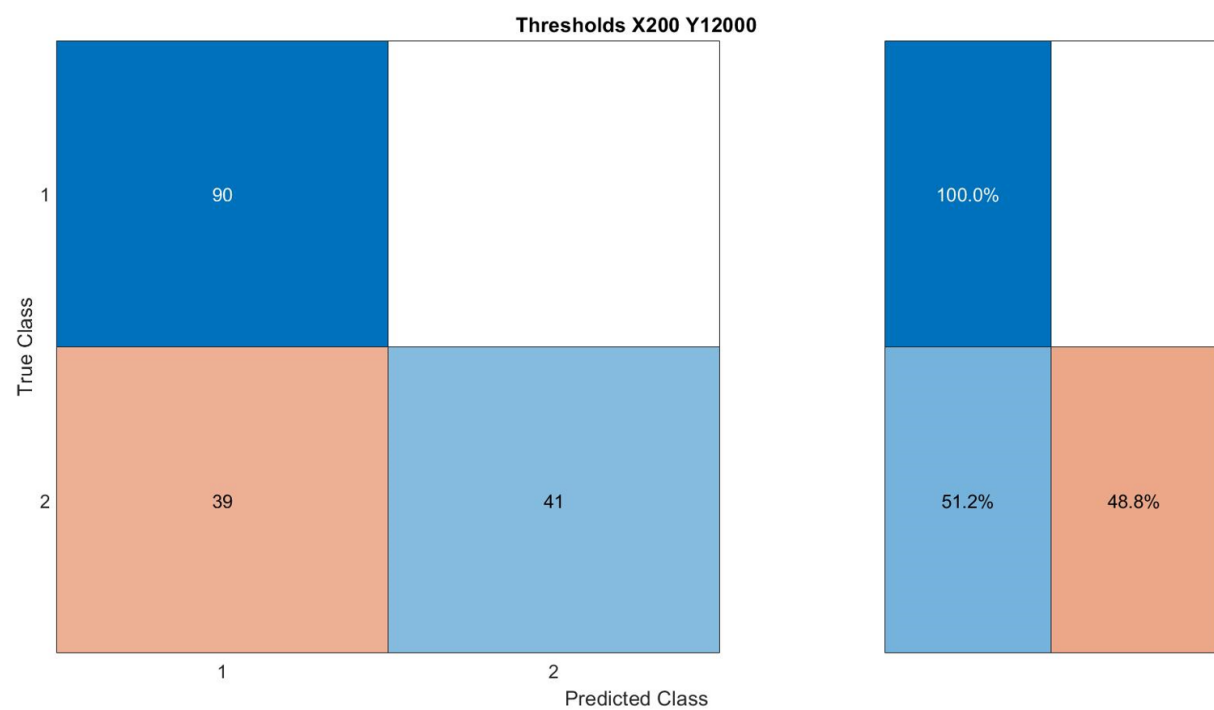


*Figure 73: Confusion matrix of thresholds X200 Y12000*

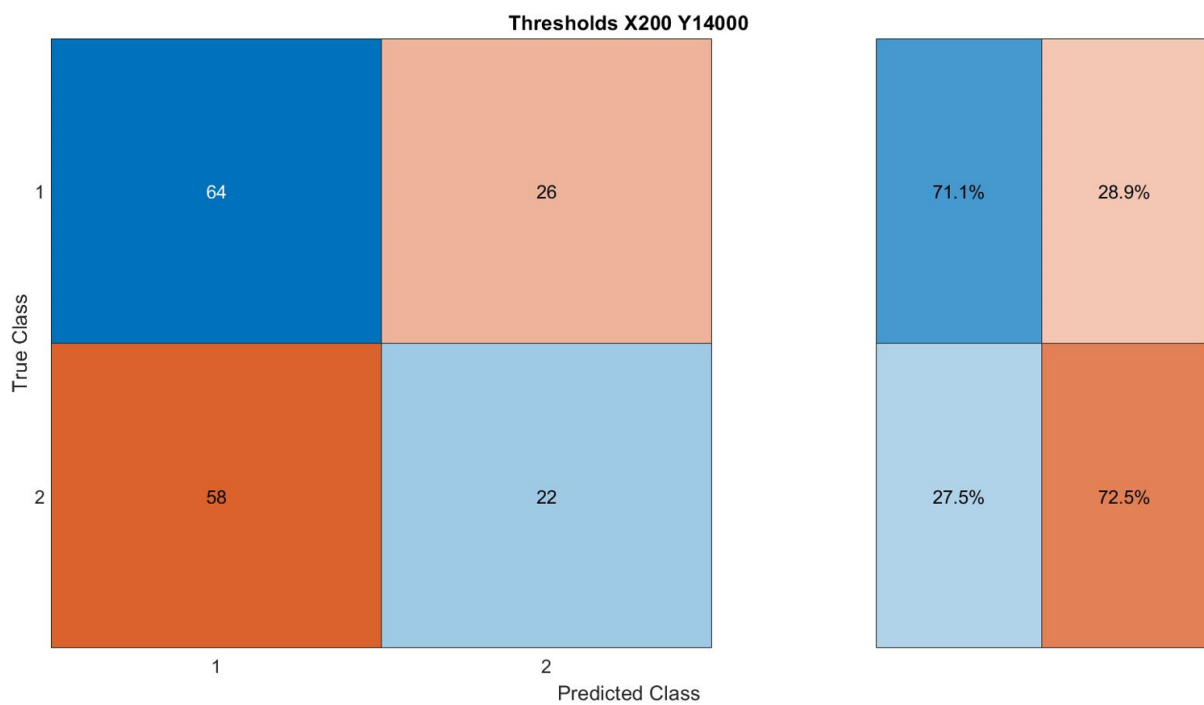


**Figure 74:** Confusion matrix of thresholds X200 Y14000



**Figure 75:** Threshold measurement 2&3 Saboor



**Figure 76:** Threshold measurement 2&3 Tobias

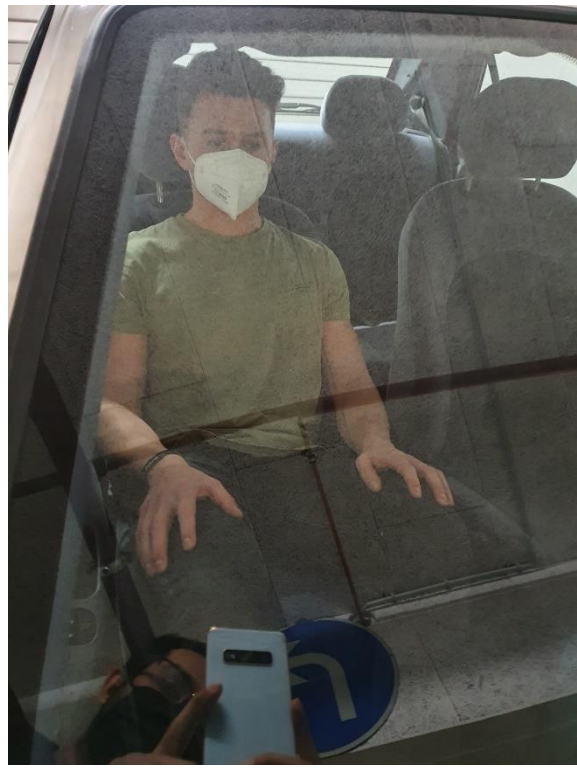


*Figure 77: Threshold measurement 2&3 Sascha*

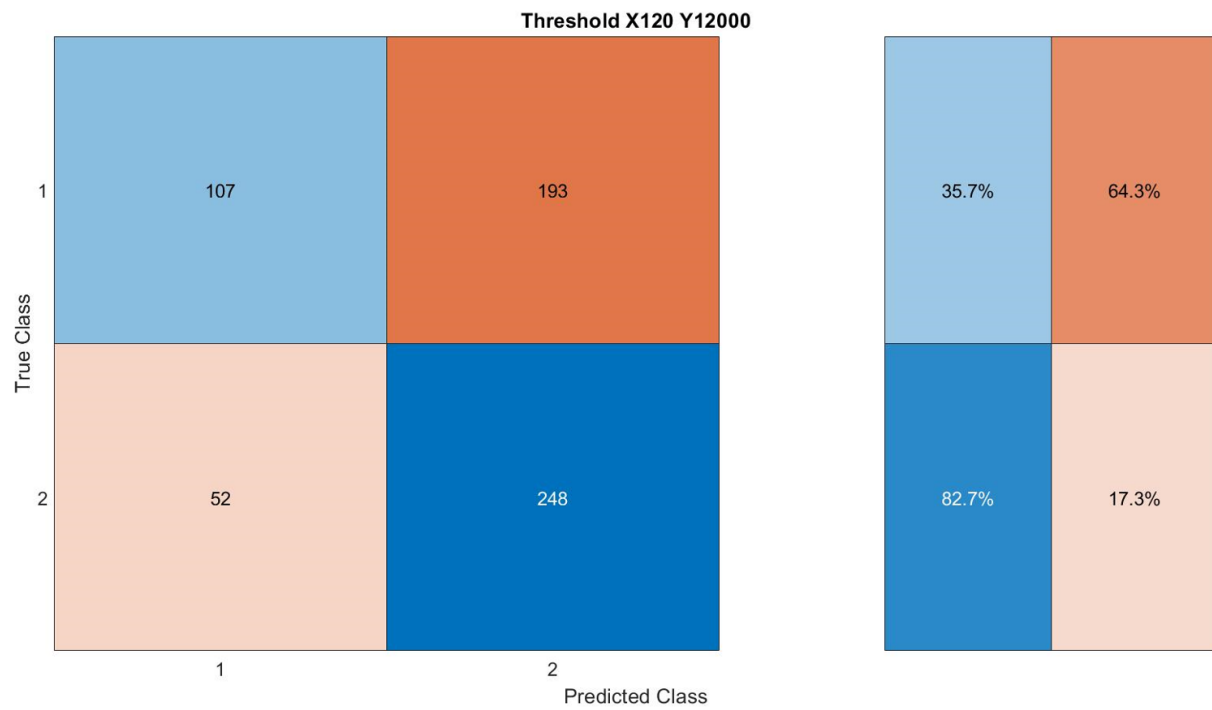


*Figure 78: Confusion matrix of thresholds X120 Y12000*

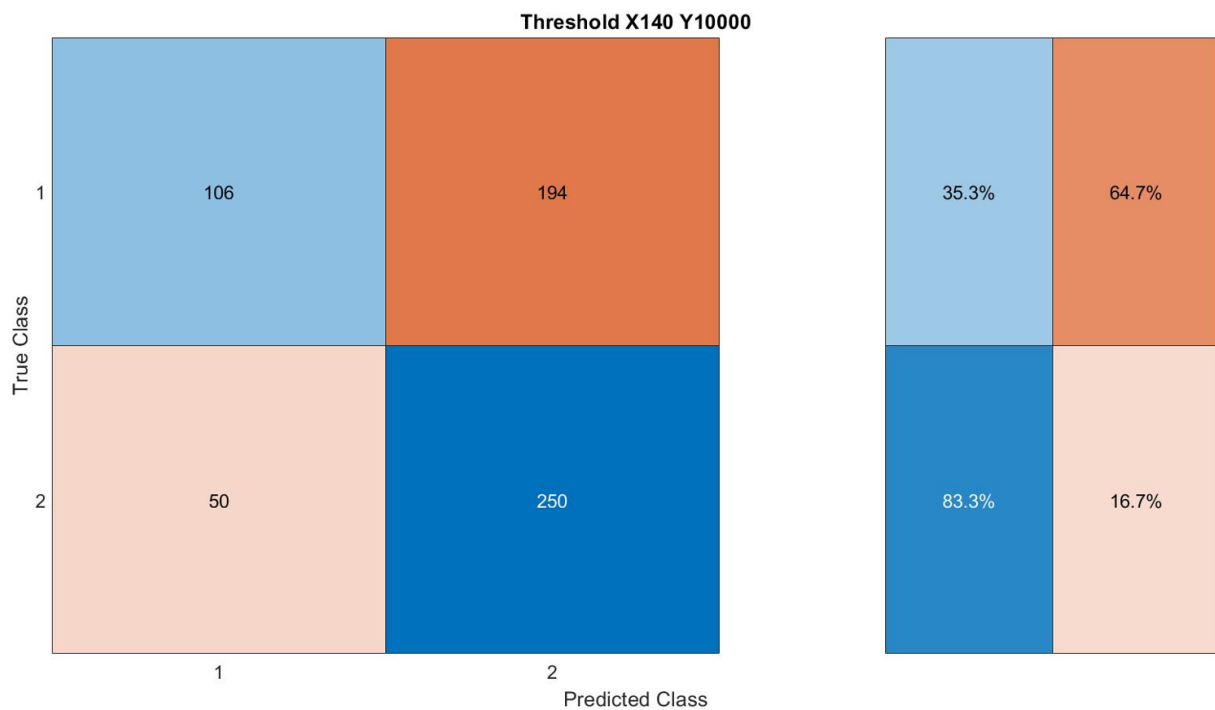


*Figure 79: Confusion matrix of thresholds X140 Y10000*

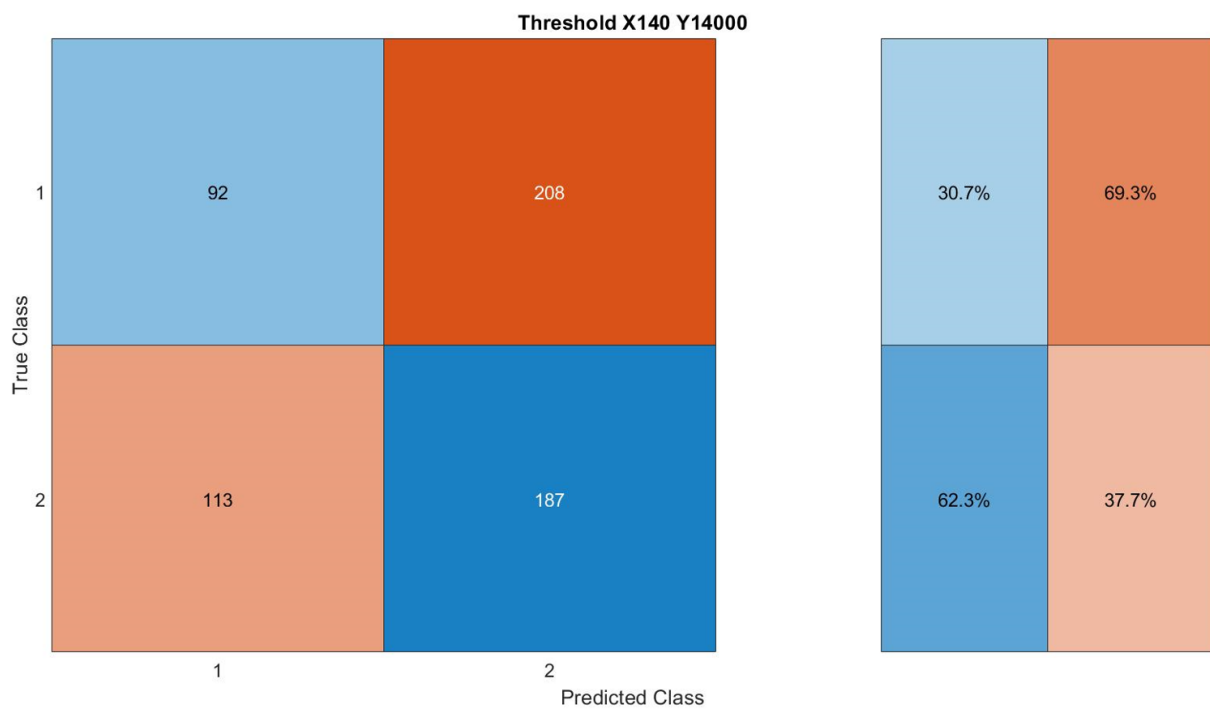


*Figure 80: Confusion matrix of thresholds X140 Y14000*

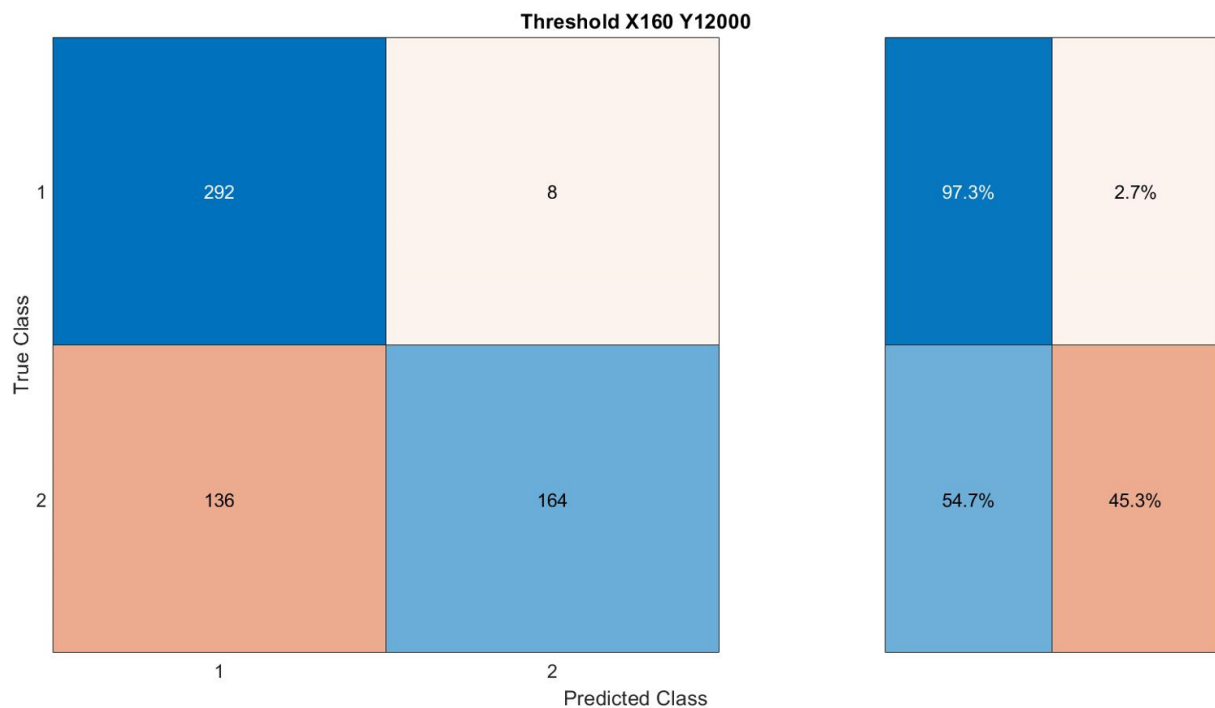


*Figure 81:* Confusion matrix of thresholds X160 Y12000

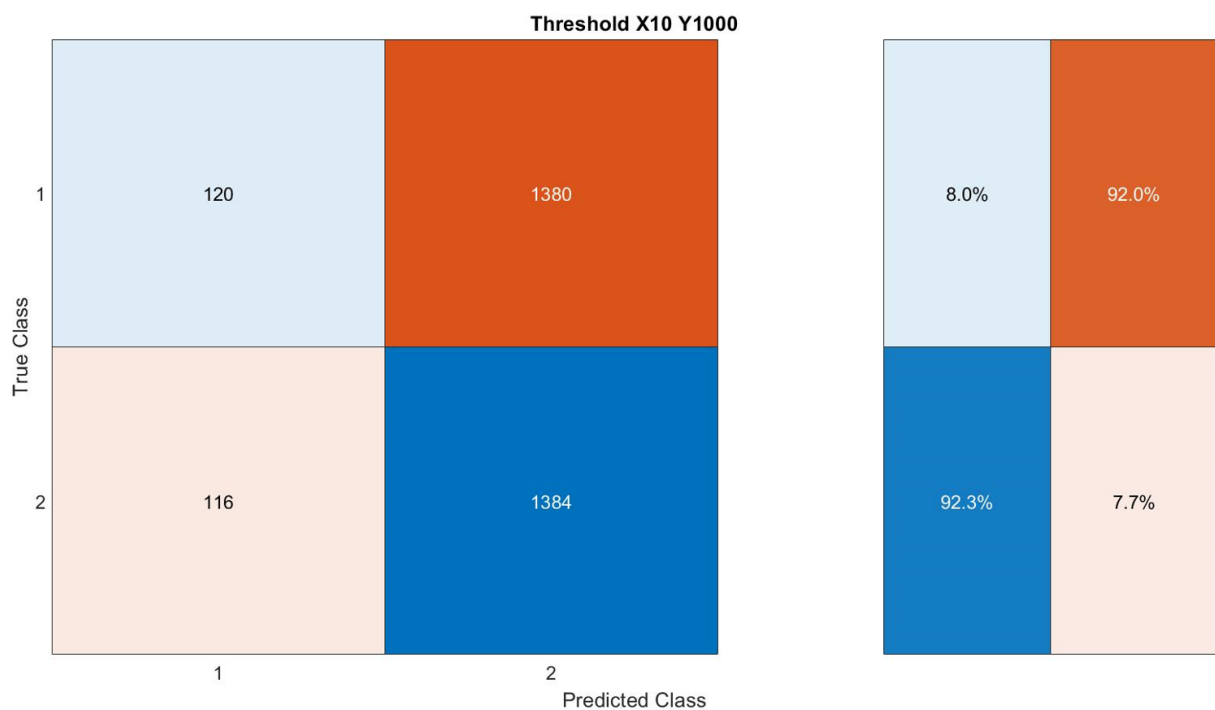


*Figure 82:* Confusion matrix of thresholds X10 Y1000

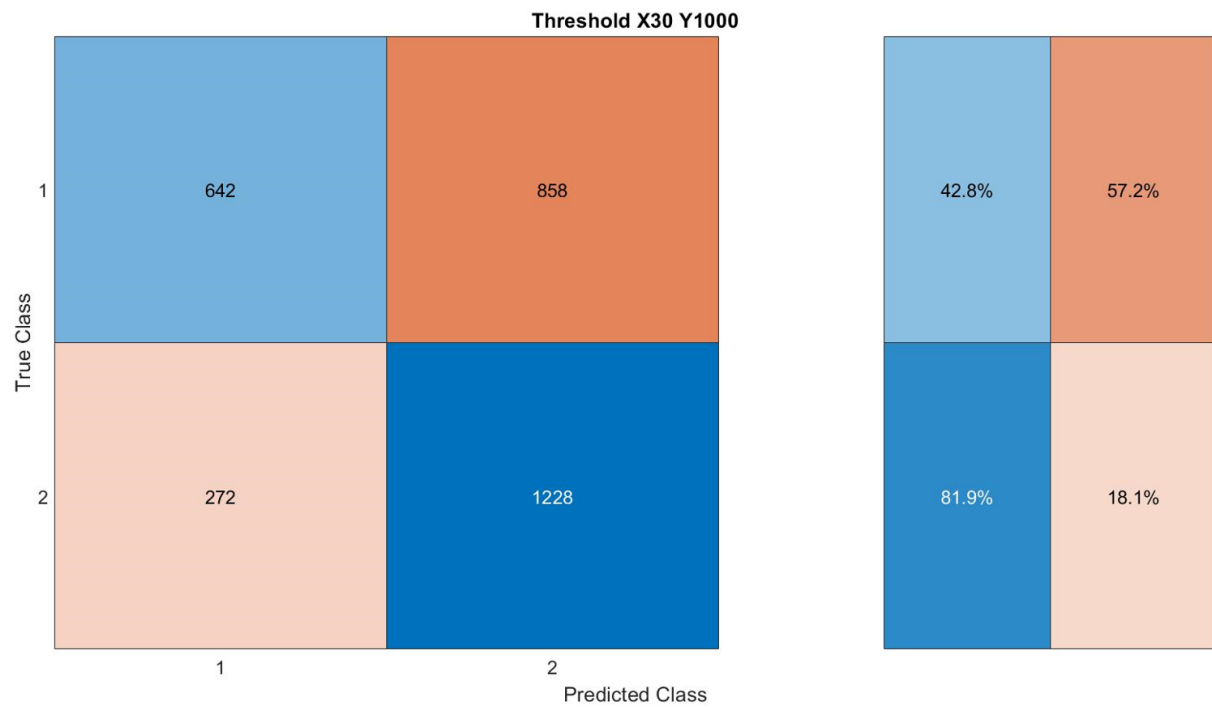


*Figure 83: Confusion matrix of thresholds X30 Y1000*

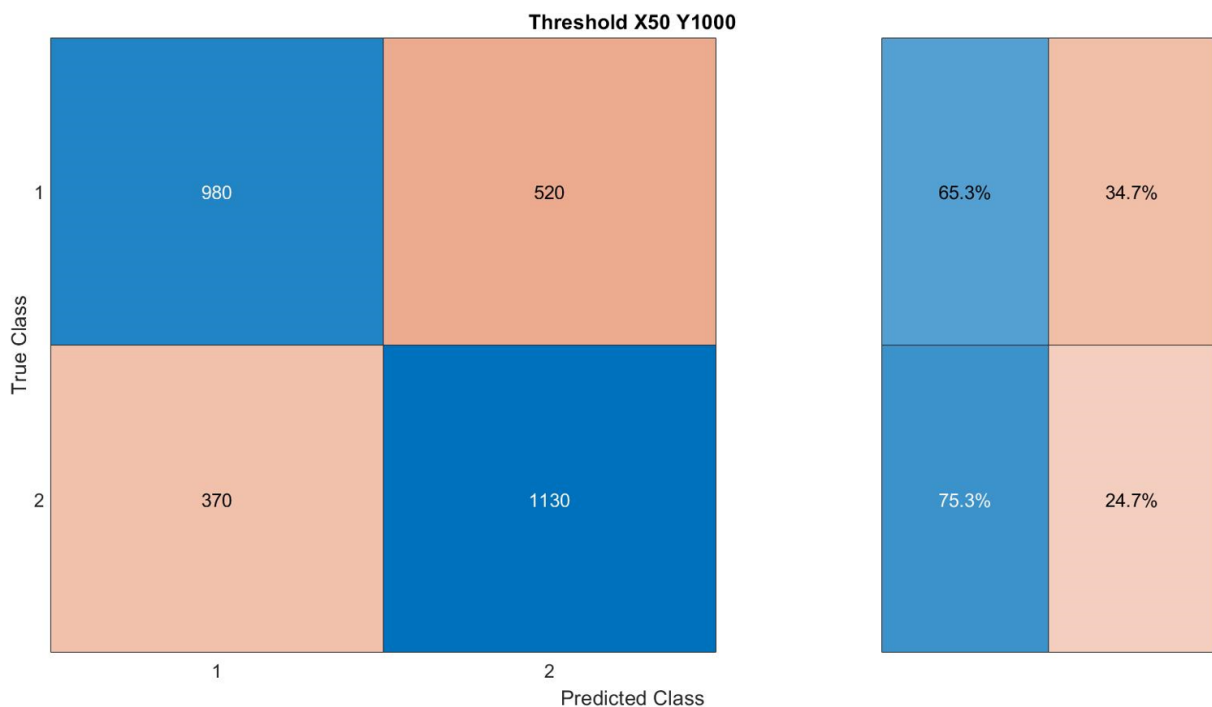


*Figure 84: Confusion matrix of thresholds X50 Y1000*

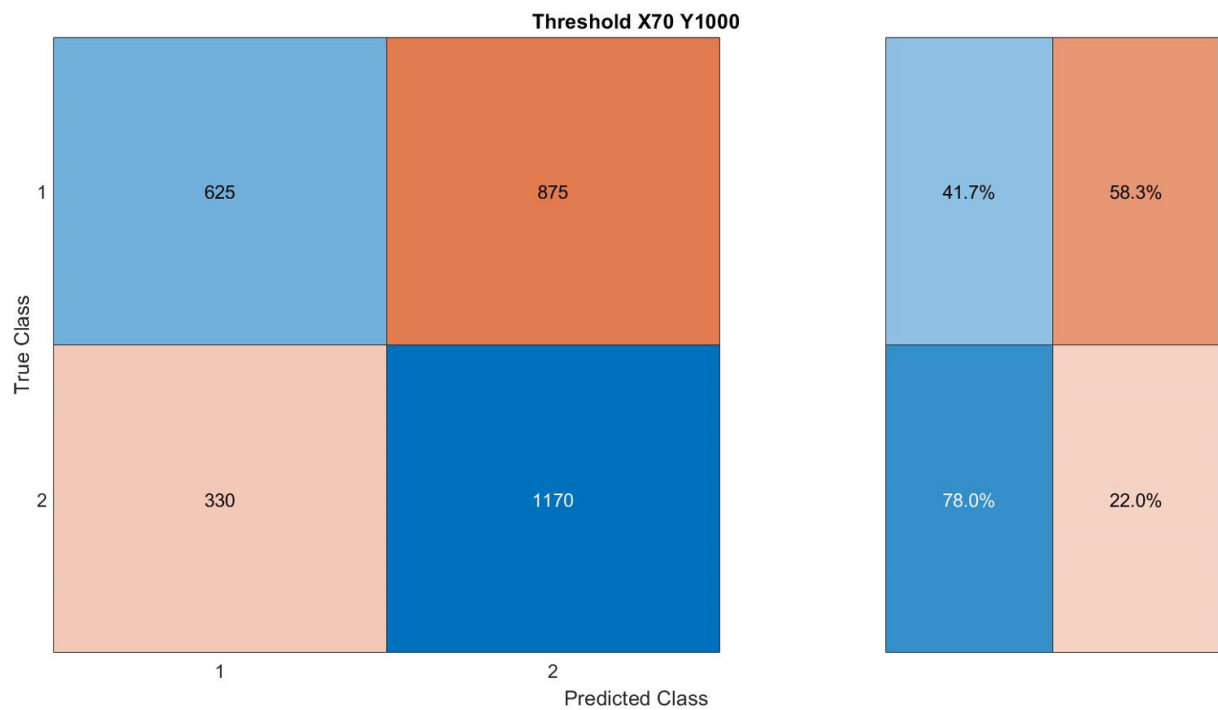


*Figure 85: Confusion matrix of thresholds X70 Y1000*

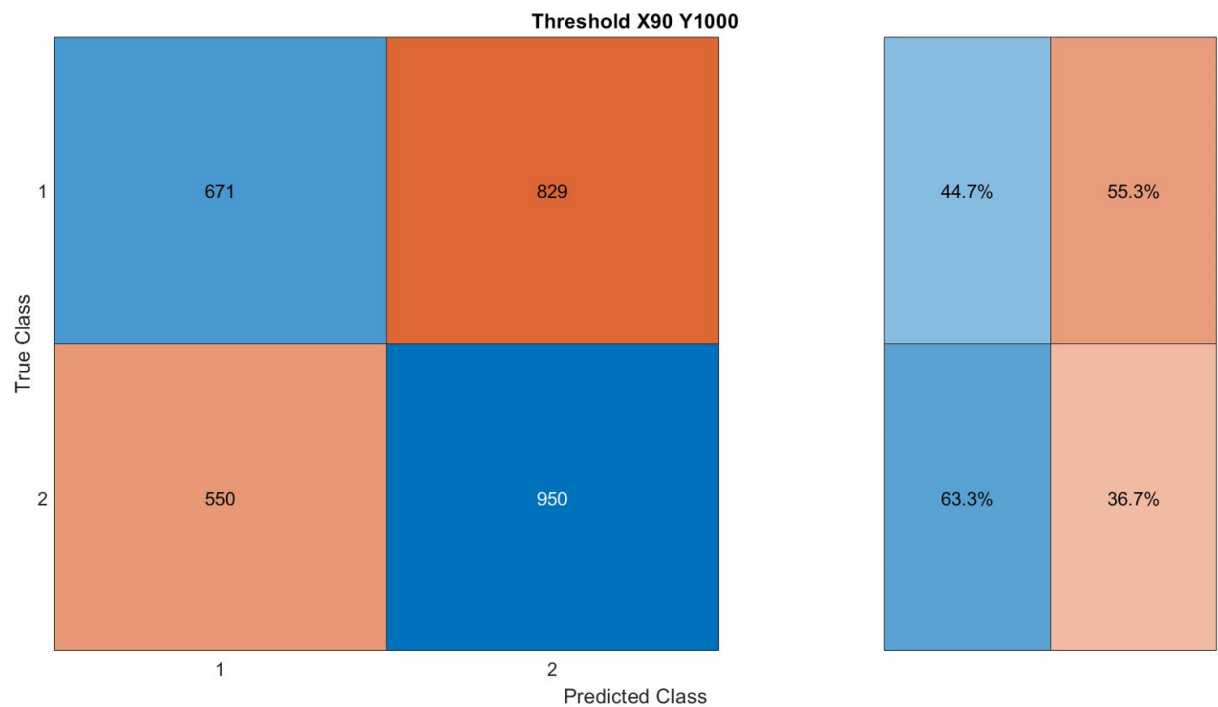


*Figure 86: Confusion matrix of thresholds X90 Y1000*

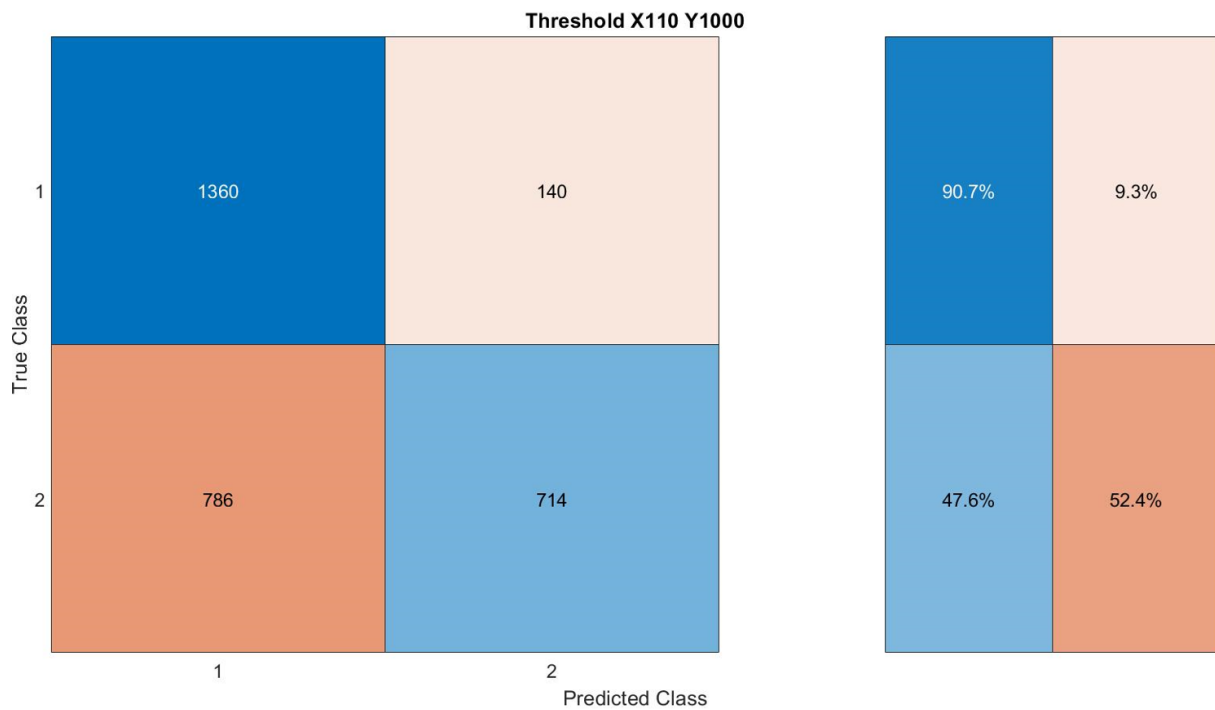


*Figure 87: Confusion matrix of thresholds X110 Y1000*

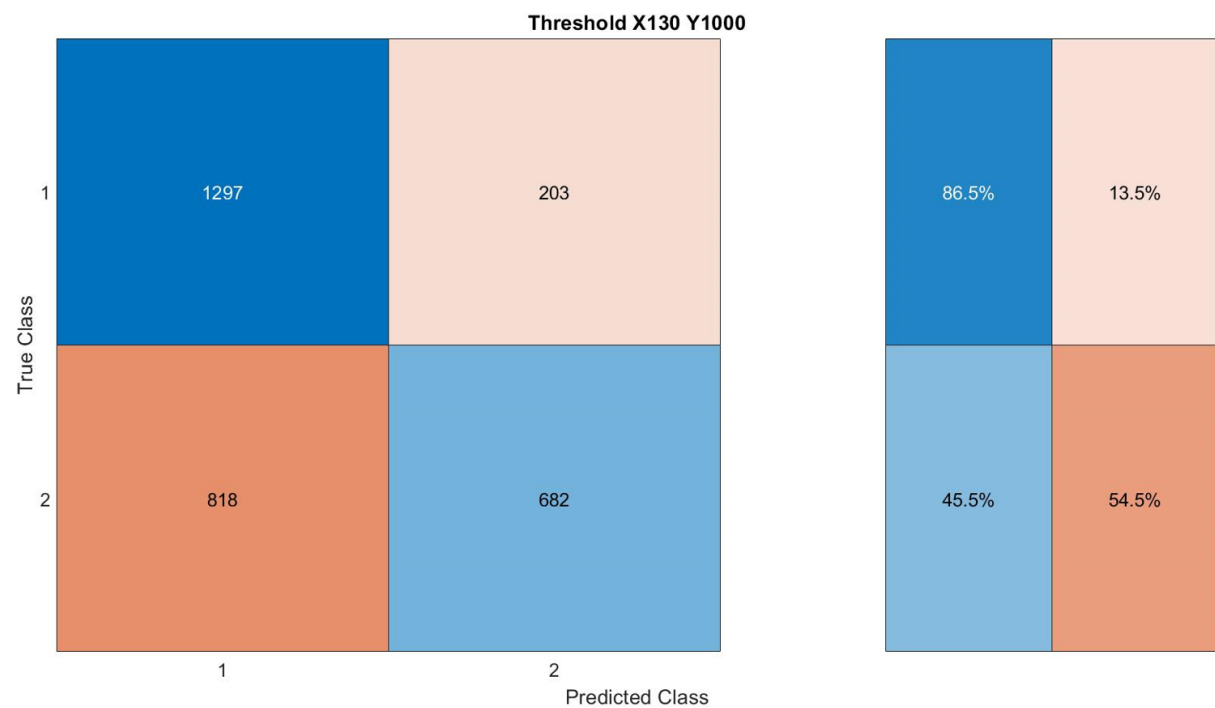


*Figure 88: Confusion matrix of thresholds X130 Y1000*

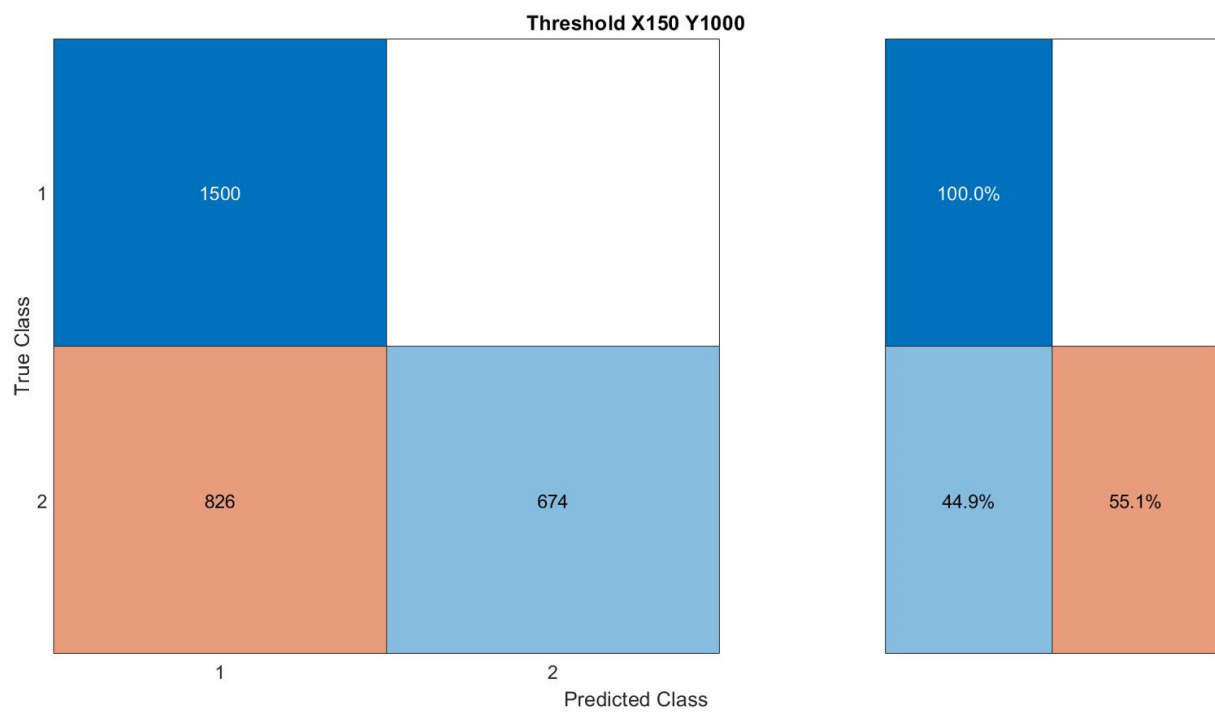


*Figure 89: Confusion matrix of thresholds X150 Y1000*

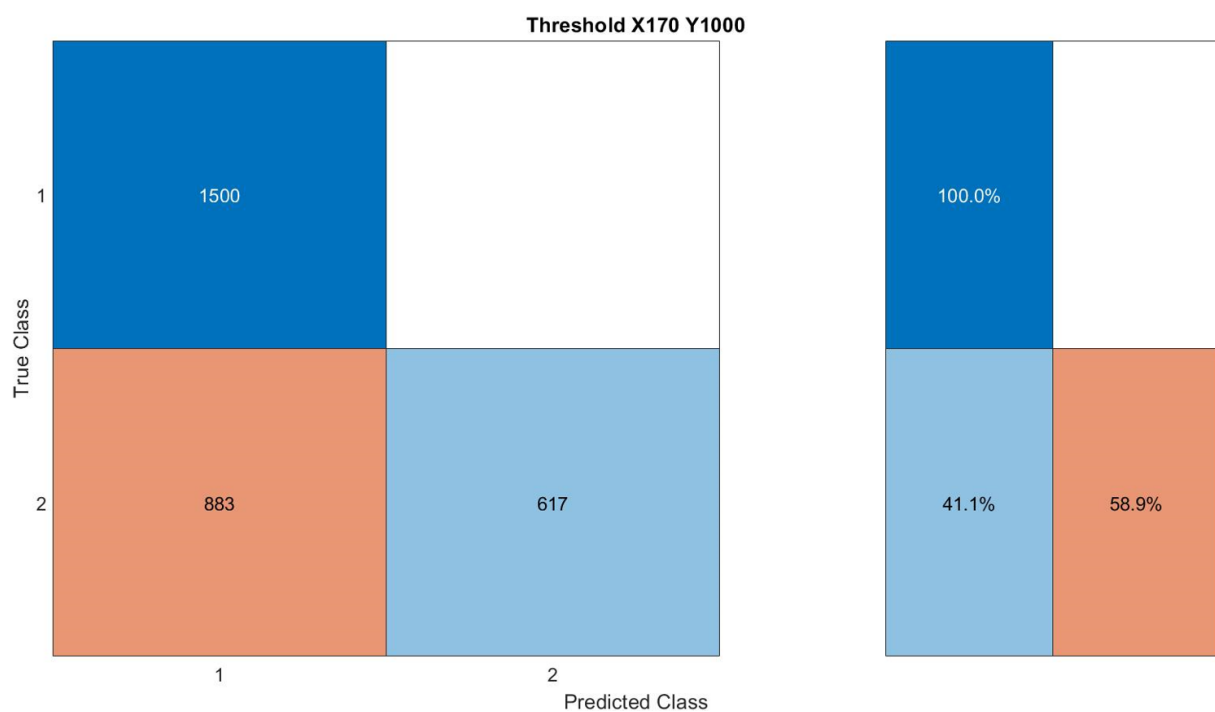


*Figure 90: Confusion matrix of thresholds X170 Y1000*

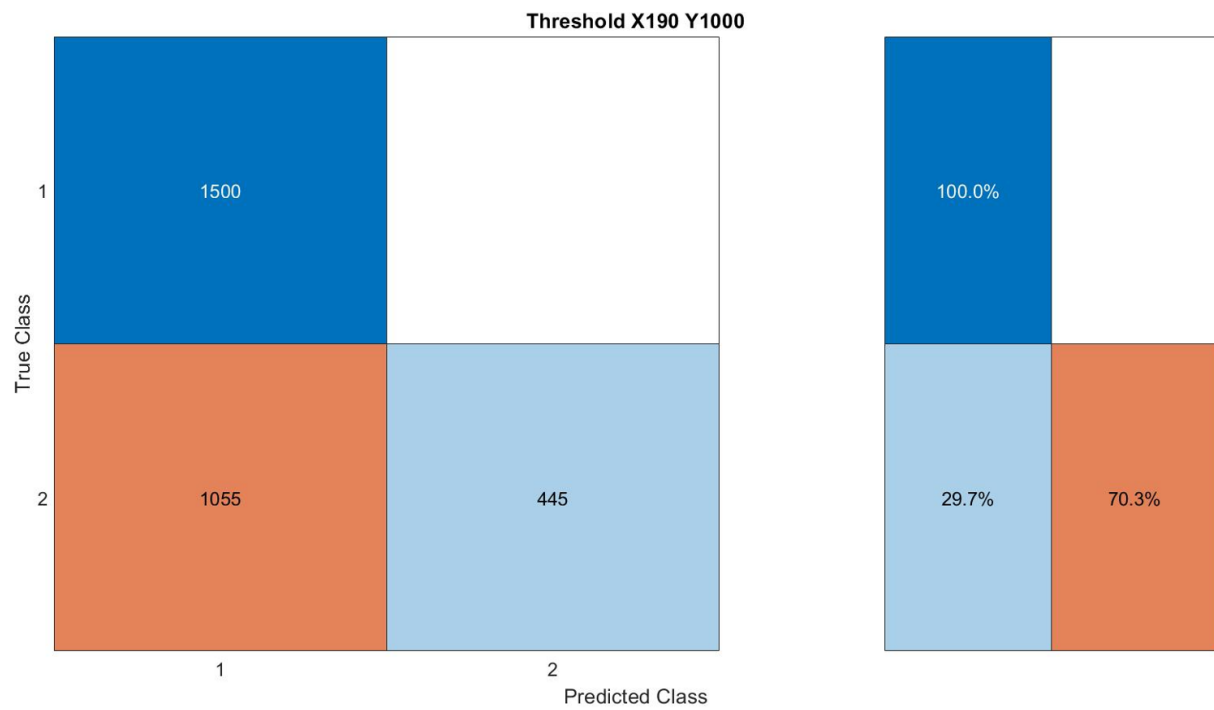


*Figure 91: Confusion matrix of thresholds X190 Y1000*

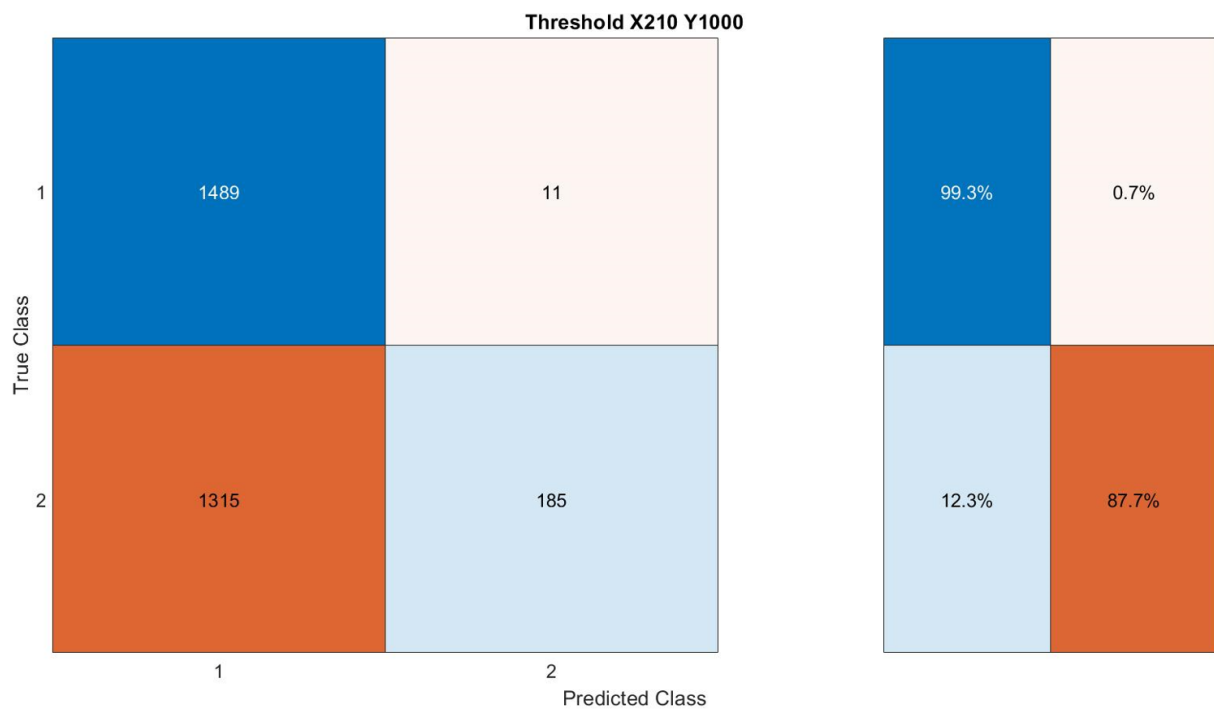


*Figure 92: Confusion matrix of thresholds X210 Y1000*

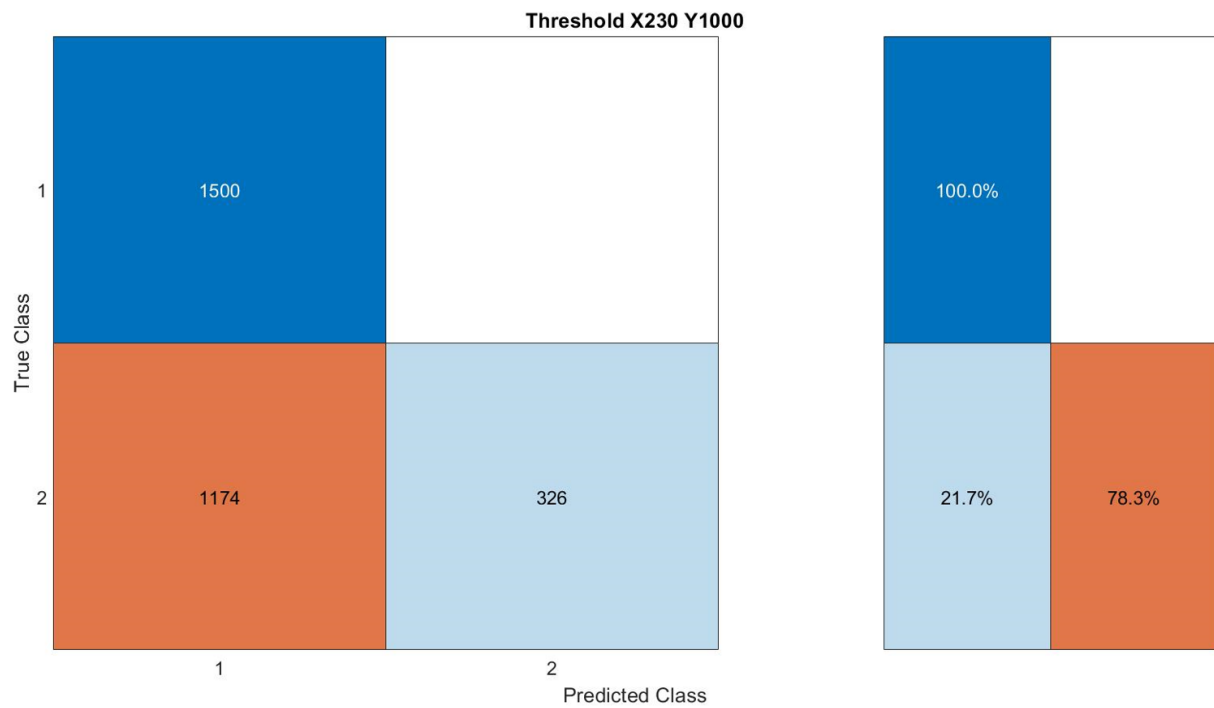


*Figure 93: Confusion matrix of thresholds X230 Y1000*

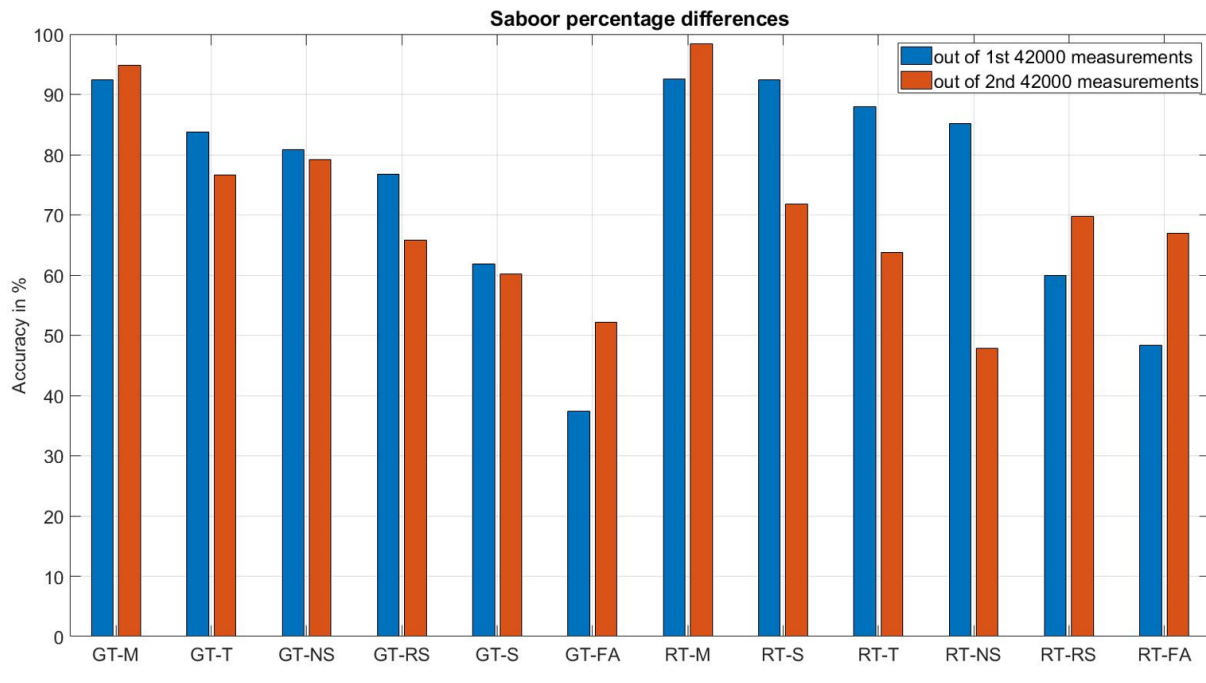


*Figure 94: Percentage differences of events between the data sets Saboor*

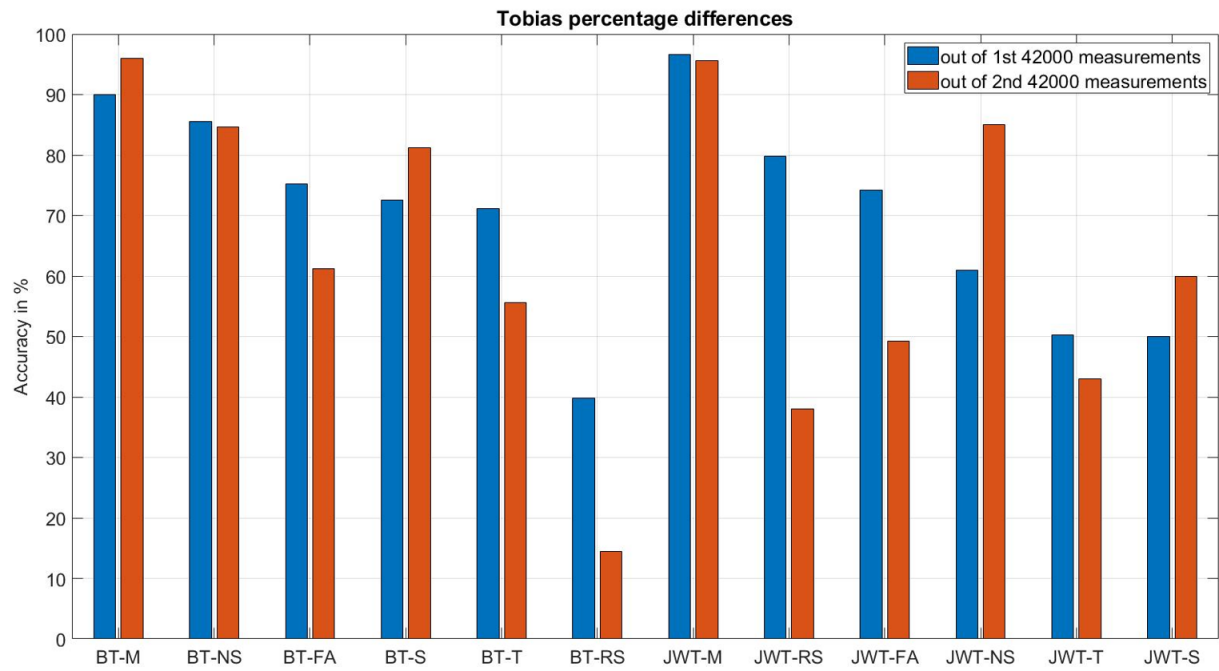


*Figure 95: Percentage differences of events between the data sets Tobias (Part 1)*

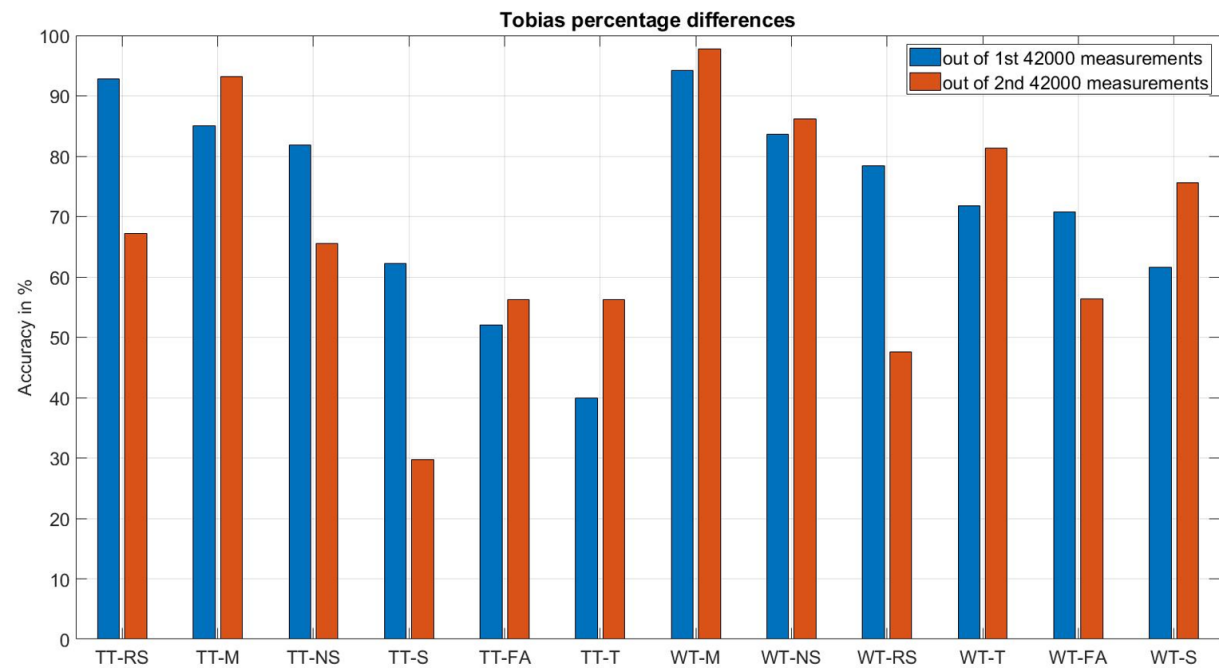


*Figure 96: Percentage differences of events between the data sets Tobias (Part 2)*

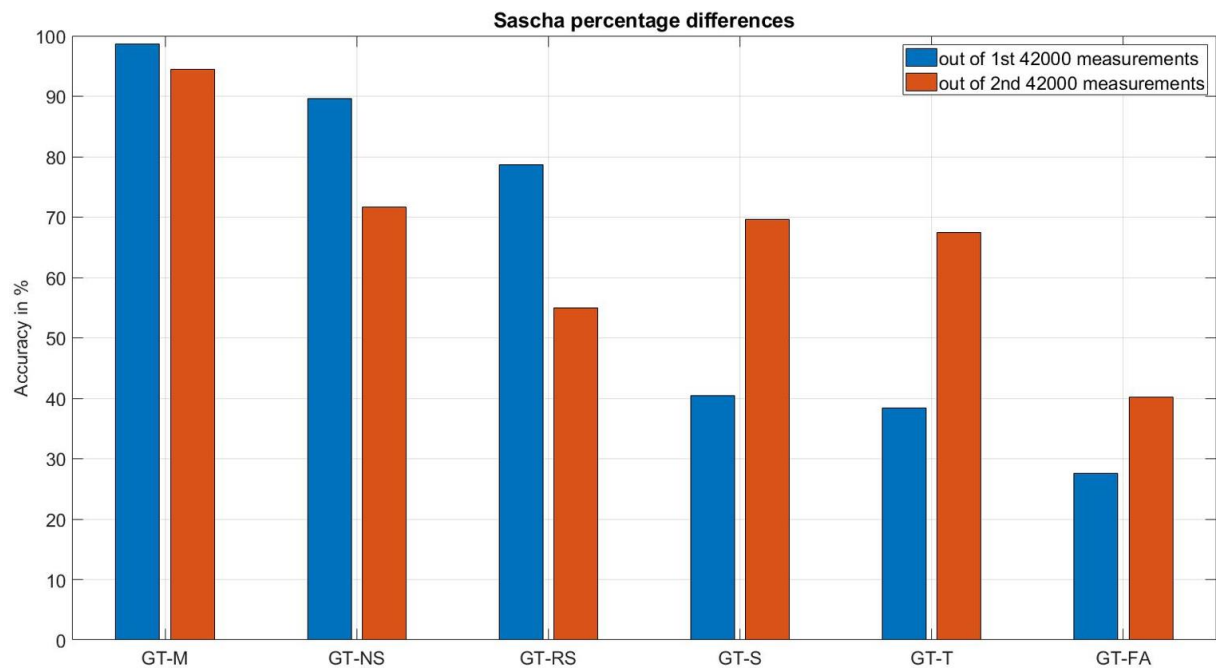


*Figure 97: Percentage differences of events between the data sets Sascha*



*Figure 98: Empty SPF SF*



*Figure 99: Empty SPF SN*



**Figure 100:** Empty SPF SB



**Figure 101:** Empty SPB SF



**Figure 102:** Empty SPB SN

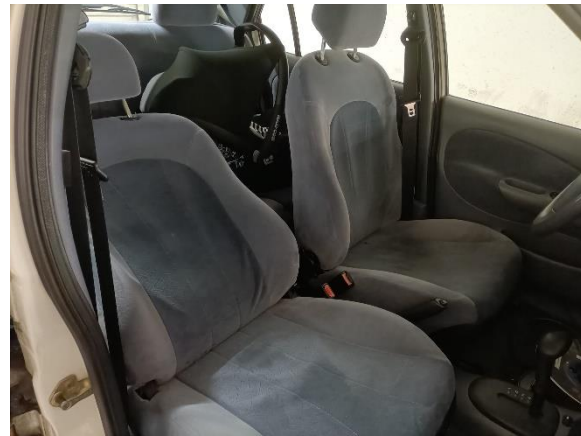


**Figure 103:** Empty SPB SB



**Figure 104:** Tobias SPF SF



**Figure 105:** Tobias SPF SN



**Figure 106:** Tobias SPF SB



**Figure 107:** Tobias SPB SF



*Figure 108: Tobias SPB SN*



*Figure 109: Tobias SPB SB*



*Figure 110: Sascha SPF SF*



*Figure 111: Sascha SPF SN*



*Figure 112: Sascha SPF SB*



*Figure 113: Sascha SPF SN*



*Figure 114: Sascha SPB SN*



*Figure 115: Sascha SPB SB*



*Figure 116: Confusion matrix of SPF SF sensor 1*



*Figure 117: Confusion matrix of SPF SN sensor 1*

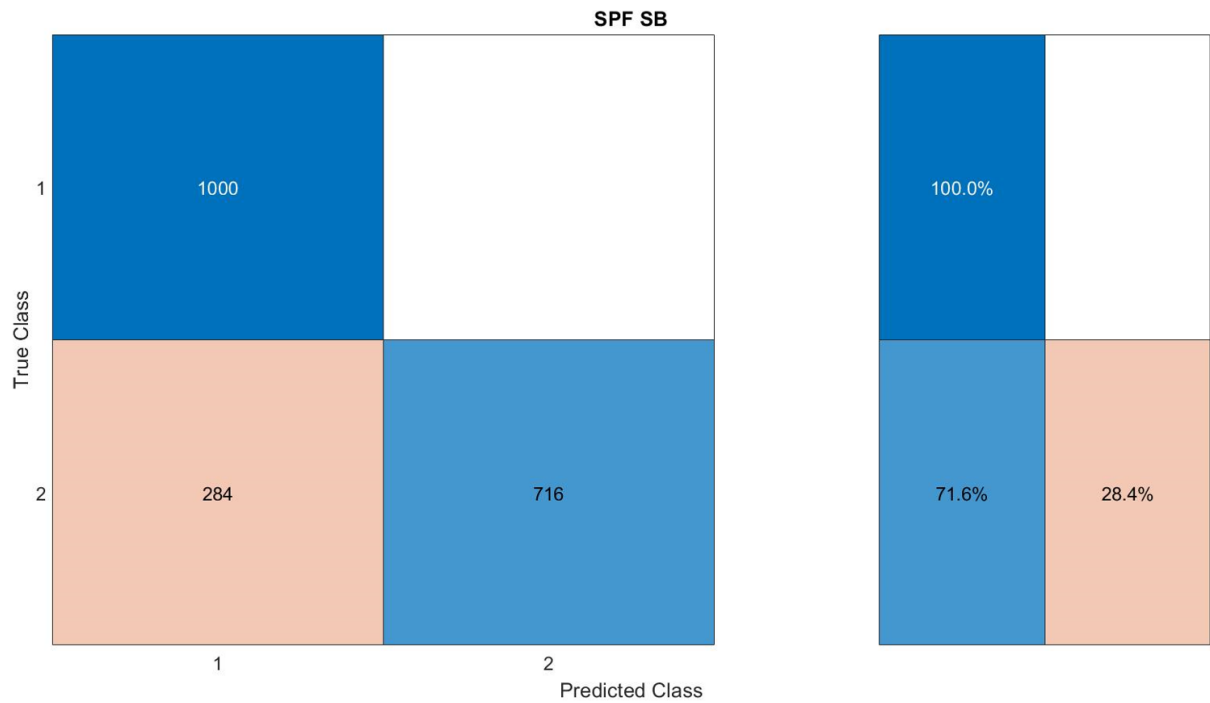


**Figure 118:** Confusion matrix of SPF SB sensor 1

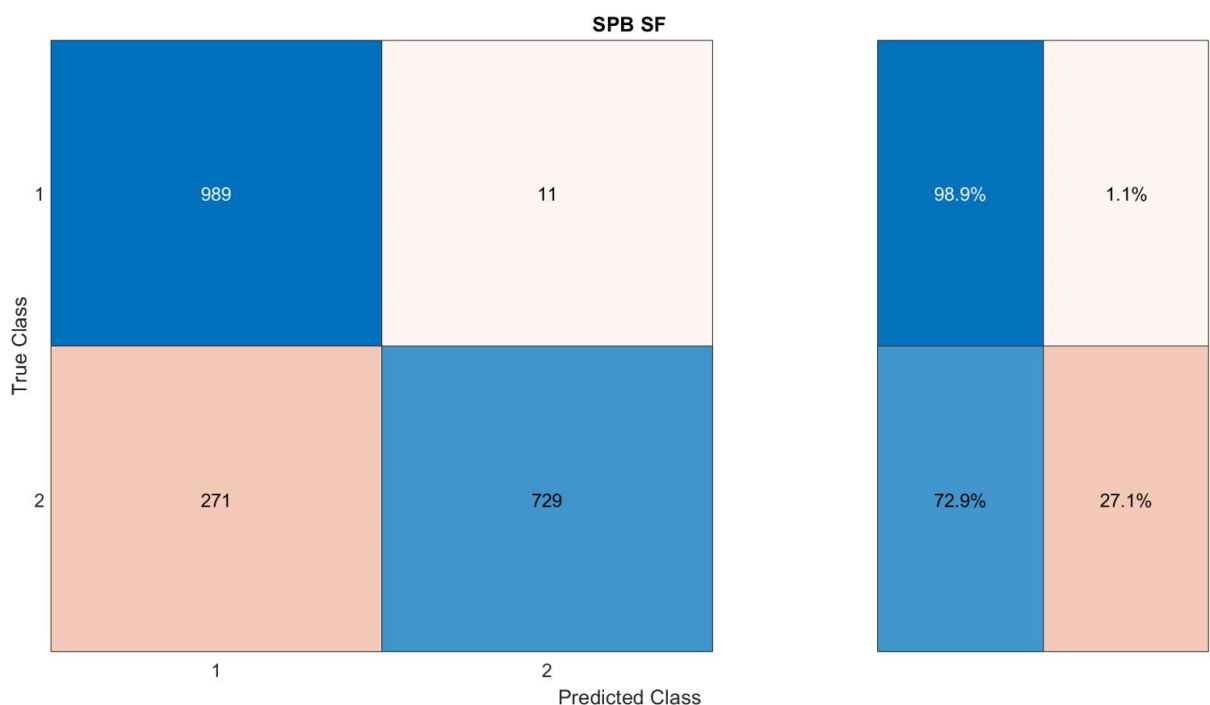


**Figure 119:** Confusion matrix of SPB SF sensor 1

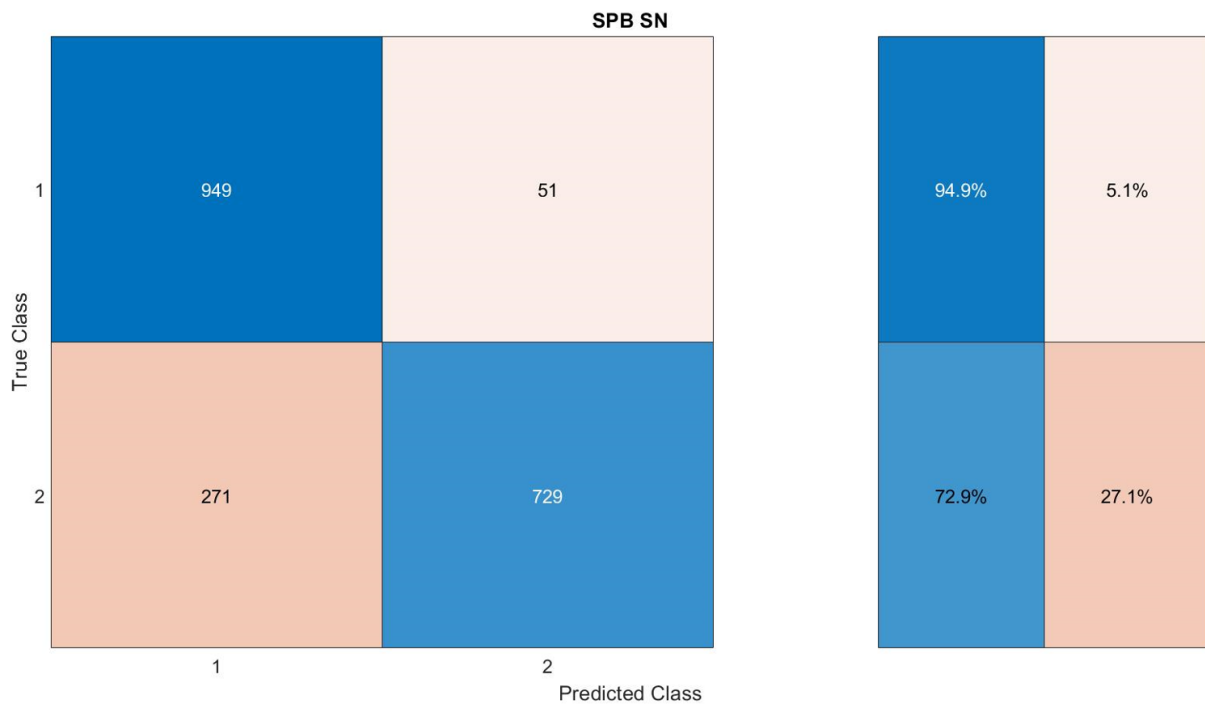


*Figure 120: Confusion matrix of SPB SN sensor 1*



*Figure 121: Confusion matrix of SPB SB sensor 1*

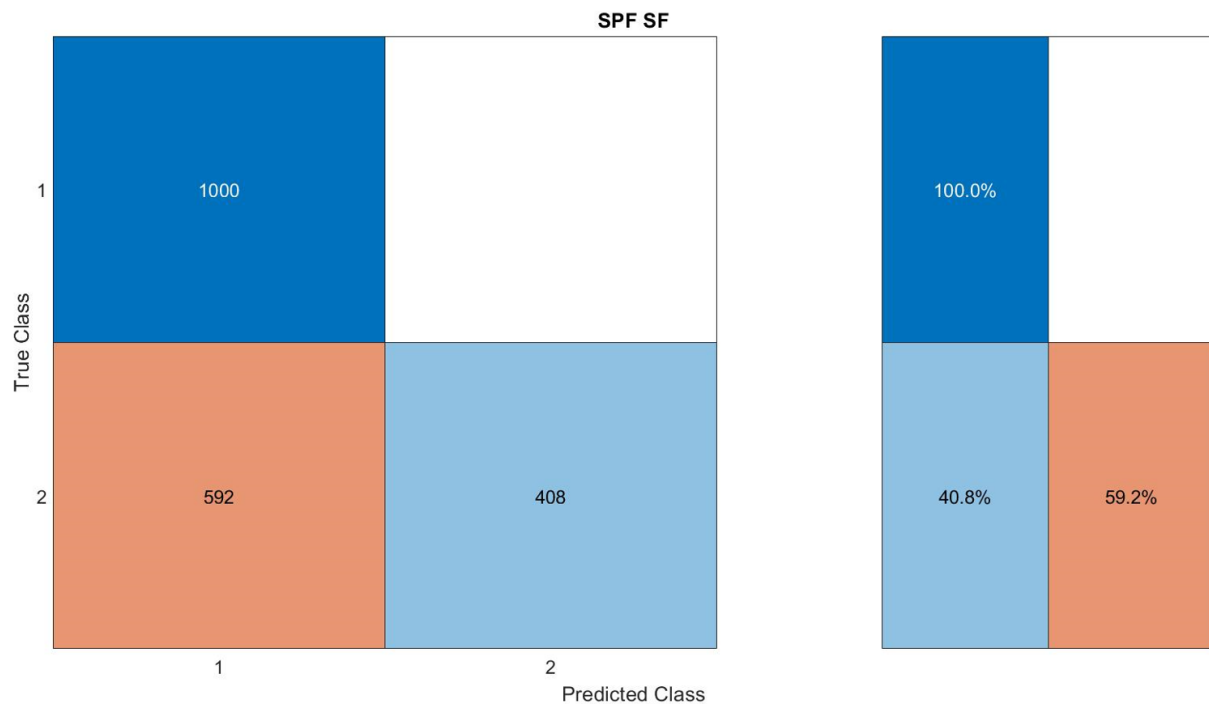


**Figure 122:** Confusion matrix of SPF SF sensor 2



**Figure 123:** Confusion matrix of SPF SN sensor 2

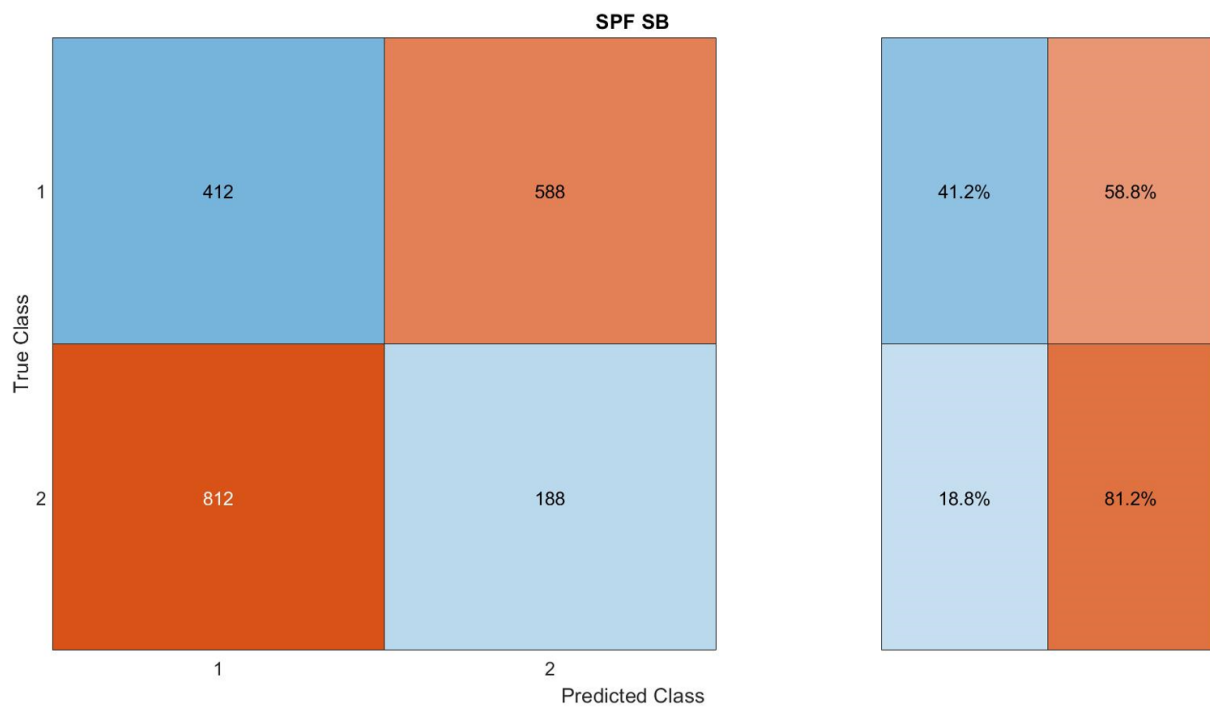


*Figure 124: Confusion matrix of SPF SB sensor 2*



*Figure 125: Confusion matrix of SPB SF sensor 2*

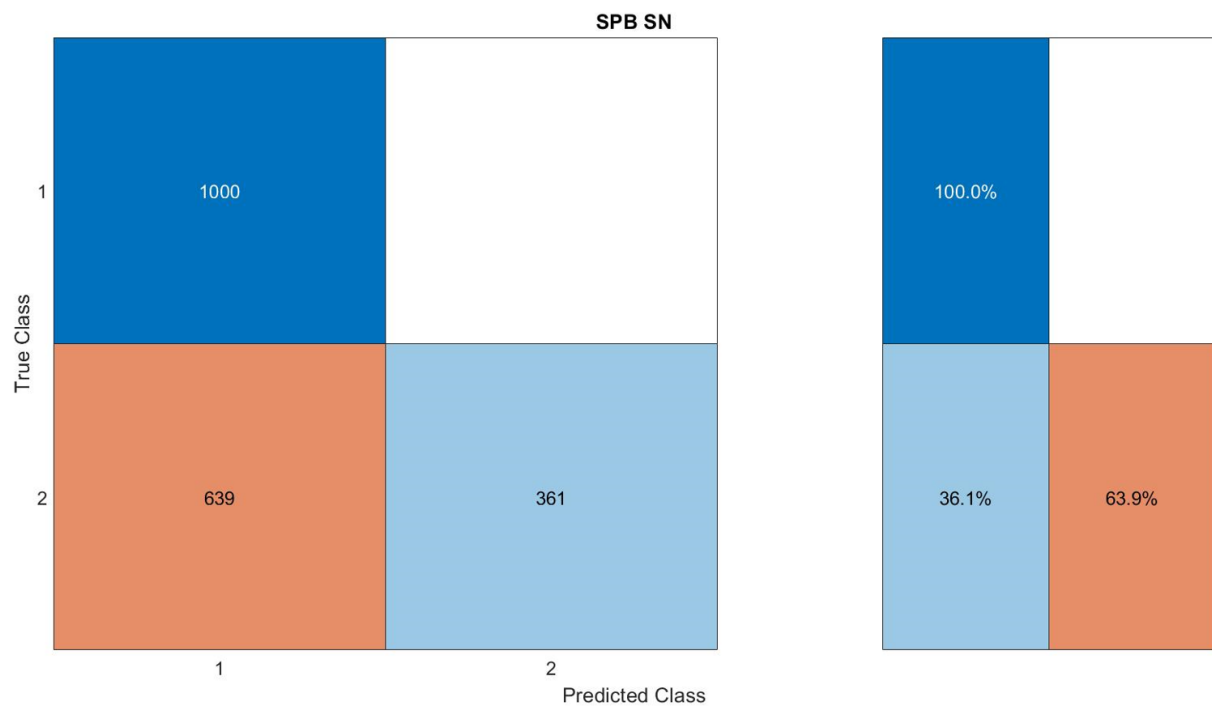


*Figure 126: Confusion matrix of SPB SN sensor 2*

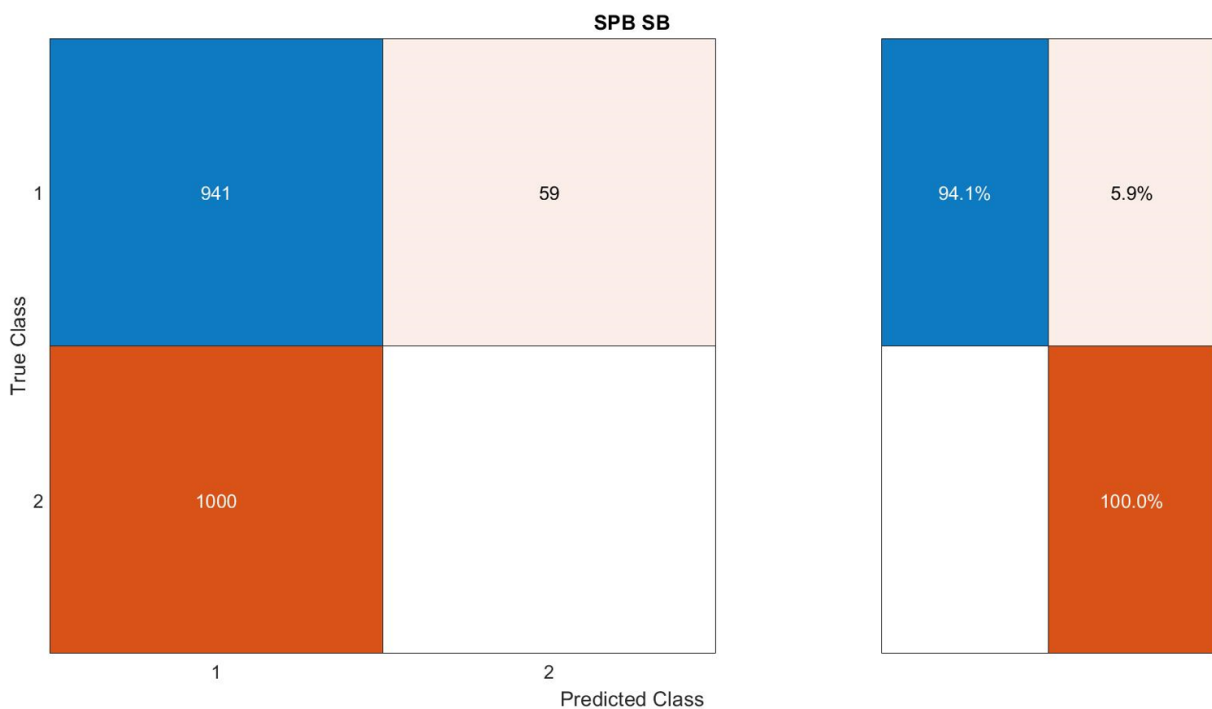


*Figure 127: Confusion matrix of SPB SB sensor 2*



*Figure 128: Plastic Baby*



*Figure 129: Backpack 1*



*Figure 130: Backpack 2*



*Figure 131: Cardboard box*



**Figure 132:** Traffic cones

**Table 12:** Comparison of the 25 classifiers

Classifier	ACCVAL [%]	ACCTEST [%]	PS [ $\mu$ s/Pred.]	Tt [s]	MS [MB]
Coarse Gaussian SVM	95.20%	96.10%	18.52	21.66	0.834
Medium NN	97.70%	95.10%	0.67	98.82	0.013
Coarse KNN	96.20%	94.30%	14.49	3.09	5.214
Fine KNN	97.20%	93.20%	2.17	0.88	5.214
Weighted KNN	97.50%	92.50%	4.55	1.34	5.214
Narrow NN	96.90%	89.90%	0.77	58.34	0.01
Medium Gaussian SVM	96.80%	89.40%	8.33	15.83	0.494
Trilayered NN	97.80%	88.70%	0.67	120.55	0.016
Bilayered NN	97.70%	88.30%	0.63	86.93	0.013
Bagged Trees	97.90%	87.90%	9.09	11.37	4.788
Wide NN	97.90%	87.60%	1	405.17	0.027
Medium KNN	97.20%	87.30%	4.55	1.42	5.214
Kernel Naive Bayes	95.50%	87.20%	1408.45	249.56	9.15
Cubic KNN	97.30%	86.40%	19.23	4.03	5.215
Subspace KNN	96.90%	83.60%	20.83	10.56	96.874
Subspace Discriminant	92.40%	81.80%	9.09	4.48	0.08
Cosine KNN	97.20%	81.20%	35.71	6.78	4.726
Linear Discriminant	92.60%	80.40%	0.83	1.19	0.008
Boosted Trees	96.80%	78.00%	5.88	7.85	0.287
Fine Tree	96.60%	77.80%	0.53	1.4	0.028
Gaussian Naive Bayes	93.30%	76.60%	0.83	1.15	0.005
RUS Boosted Trees	95.50%	76%	4.76	8.7	0.289
Medium Tree	95.50%	76%	0.5	0.6	0.013
Quadratic Discriminant	94.20%	75.90%	0.71	0.94	0.011
Coarse Tree	92.40%	75.40%	0.48	0.48	0.007
Fine Gaussian SVM	97.90%	69.30%	9.09	25.99	0.611